Biomaterials Science

ROYAL SOCIETY OF CHEMISTRY

REVIEW

View Article Online
View Journal | View Issue

Cite this: *Biomater. Sci.*, 2025, **13**, 1131

Integrating microfluidics, hydrogels, and 3D bioprinting for personalized vessel-on-a-chip platforms

San Seint Seint Aye, [a] Zhongqi Fang,[a] Mike C. L. Wu,[a,b] Khoon S. Lim *[b,c] and Lining Arnold Ju *[a,b,d,e]

Thrombosis, a major cause of morbidity and mortality worldwide, presents a complex challenge in cardiovascular medicine due to the intricacy of clotting mechanisms in living organisms. Traditional research approaches, including clinical studies and animal models, often yield conflicting results due to the inability to control variables in these complex systems, highlighting the need for more precise investigative tools. This review explores the evolution of *in vitro* thrombosis models, from conventional polydimethylsiloxane (PDMS)-based microfluidic devices to advanced hydrogel-based systems and cutting-edge 3D bioprinted vascular constructs. We discuss how these emerging technologies, particularly vessel-on-a-chip platforms, are enabling researchers to control previously unmanageable factors, thereby offering unprecedented opportunities to pinpoint specific clotting mechanisms. While PDMS-based devices offer optical transparency and fabrication ease, their inherent limitations, including non-physiological rigidity and surface properties, have driven the development of hydrogel-based systems that better mimic the extracellular matrix of blood vessels. The integration of microfluidics with biomimetic materials and tissue engineering approaches has led to the development of sophisticated models capable of simulating patient-specific vascular geometries, flow dynamics, and cellular interactions under highly controlled conditions. The advent of 3D bioprinting further enables the creation of complex, multi-layered vascular structures with precise spatial control over geometry and cellular composition. Despite significant progress, challenges remain in achieving long-term stability, incorporating immune components, and translating these models to clinical applications. By providing a comprehensive overview of current advancements and future prospects, this review aims to stimulate further innovation in thrombosis research and accelerate the development of more effective, personalized approaches to thrombosis prevention and treatment.

Received 12th October 2024,
Accepted 31st December 2024

DOI: 10.1039/d4bm01354a

rsc.li/biomaterials-science

1. Introduction

Thrombosis, the formation of blood clots within blood vessels, is a major cause of morbidity and mortality worldwide, playing a central role in various cardiovascular diseases, including myocardial infarction, stroke, and venous thromboembolism. The blood clot formed primarily consists of fibrin strands, red blood cells, platelets, and remnants of cholesterol.[1] Thrombosis may result in reduced blood flow to tissue due to a growing thrombus or thromboembolism caused by thrombus rupture, leading to sudden and in-hospital death from stroke, heart attack, or pulmonary embolism (Fig. 1).[2]

Understanding the complex mechanisms underlying thrombosis is crucial for developing effective preventive strategies and treatments. However, the intricate interplay between blood components, vascular endothelium, and hemodynamic factors in thrombosis presents significant challenges for researchers. The formation of blood clots within blood vessels is classically described by Virchow's triad, comprising three main factors: endothelial cell injury, hemodynamic flow disturbance, and hypercoagulability (Fig. 1).

Traditionally, thrombosis research has relied on *in vivo* animal models and *in vitro* cell culture systems. While animal models provide physiological relevance, they often fail to fully recapitulate human pathophysiology and present ethical concerns. Moreover, the U.S. Food and Drug Administration (FDA) recently announced that animal models are no longer required as pre-clinical models,[3] further emphasizing the need for

[a]*School of Biomedical Engineering, The University of Sydney, Darlington, NSW 2008, Australia. E-mail: arnold.ju@sydney.edu.au*
[b]*Charles Perkins Centre, The University of Sydney, Camperdown, NSW 2006, Australia. E-mail: khoon.lim@sydney.edu.au*
[c]*School of Medical Sciences, The University of Sydney, Camperdown, NSW 2006, Australia*
[d]*The University of Sydney Nano Institute (Sydney Nano), The University of Sydney, Camperdown, NSW 2006, Australia*
[e]*Heart Research Institute, Newtown, NSW 2042, Australia*

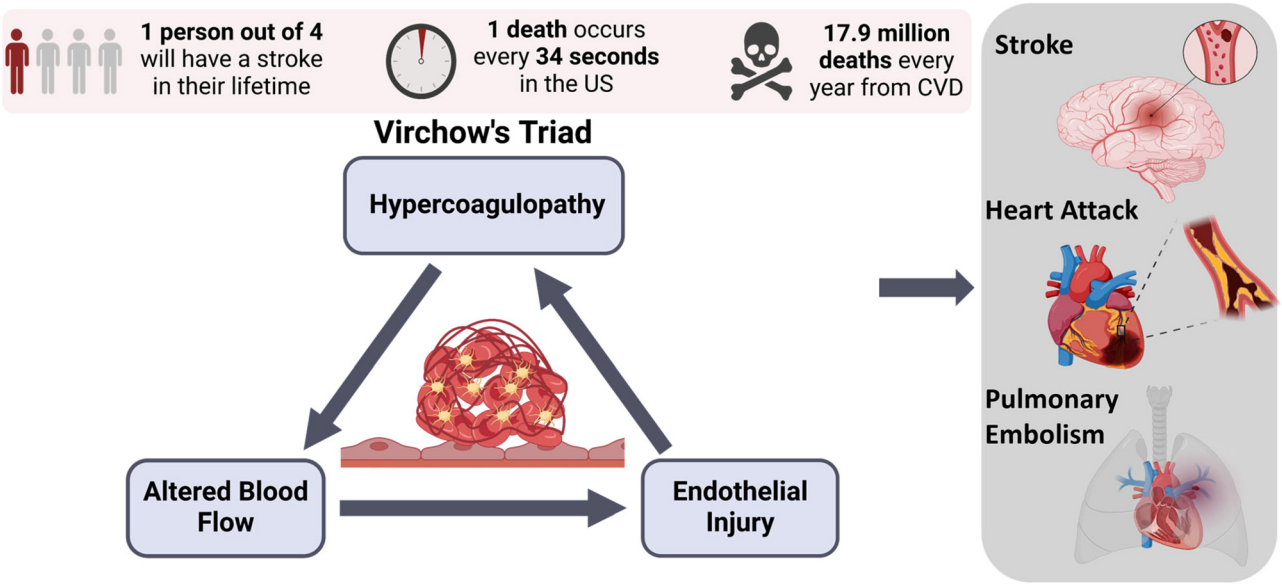

Fig. 1 Statistics of cardiovascular disease,[4–6] Virchow's triad comprising of hypercoagulopathy, altered blood flow and endothelial damage and its clinical manifestations. Figures created using Biorender (https://www.biorender.com).

alternative approaches. Conversely, conventional *in vitro* models, such as static cell cultures, lack the dynamic environment and three-dimensional architecture of blood vessels.

These limitations have spurred the development of more advanced *in vitro* models that can bridge the gap between oversimplified cell cultures and complex animal systems. To recapitulate patient-specific vascular systems with high-throughput fabrication of tailor-made vessel-on-a-chip devices that can study blood clotting outside the human body, researchers are moving beyond traditional 2D microfluidic chip models, which are limited in their ability to mimic key physiological parameters like 3D constructs, viscoelasticity, complex cell–cell crosstalk, and cell–niche interactions found in native vascular environments.[7]

In recent years, microfluidic technologies have emerged as powerful tools for studying thrombosis. These systems allow for precise control of fluid dynamics, enabling researchers to mimic physiological blood flow conditions and investigate the effects of shear stress on thrombosis.[8–12] Initially, PDMS-based microfluidic devices dominated the field, offering advantages such as optical transparency, ease of fabrication, and cost-effectiveness. However, PDMS presents several significant limitations for vascular modeling.[13–15] These include its inherent rigidity (Young's modulus ~1–3 MPa), which poorly

San Seint Seint Aye

Dr Aye is a clinician turned scientist worked in the School of Biomedical Engineering at the University of Sydney. She holds a PhD in Material Science and Engineering from Institute of Frontier Materials (IFM) at Deakin University. Her research explores biofabrication of microvascular tissues and vessel-on-a-chip technology to address on-demand vascular research and thrombosis study for cardiovascular applications. She has interests in mechanobiology combining the two emerging microfluidics and 3D bioprinting technologies.

Khoon S. Lim

Khoon S. Lim, BE (Hons 1, UNSW), ME (UNSW), PhD (UNSW) is currently an Australian Research Council Future Fellow and Associate Professor in the School of Medical Sciences at the University of Sydney. He is the co-Director of the Sydney Biomanufacturing Incubator and leads the Light Activated Biomaterials (LAB) Group. His research focuses on developing photopolymerizable hydrogel bioinks for tissue engineering and regenerative medicine applications. He is the past-President of the Australasian Society for Biomaterials and Tissue Engineering, as well as serves on the Board of Directors of the International Society for Biofabrication.

matches the mechanical properties of native blood vessels (1–500 kPa), and its high hydrophobicity, which impedes cell attachment and protein adsorption. While surface modifications through plasma treatment or coating with extracellular matrix proteins can temporarily improve cell adhesion, these modifications are often unstable and deteriorate over time. Additionally, PDMS's non-specific protein small molecule adsorption can affect experimental outcomes, particularly in drug screening applications. The material's gas permeability, while beneficial for cell culture, can lead to bubble formation in perfusion studies, and its limited ability to support three-dimensional cell culture restricts the recreation of complex vessel architectures.

Hydrogel-based microfluidic devices represent a significant advancement in this direction. By incorporating natural or synthetic hydrogels, these systems can better mimic the extracellular matrix (ECM) of blood vessels, providing a more physiologically relevant environment for cell culture. The ability to tune the mechanical and biochemical properties of hydrogels allows researchers to model various aspects of vascular physiology and pathology,[16] including endothelial barrier function,[17] cellular interactions, and thrombosis.[18,19] Hydrogels offer several advantages over PDMS, including tissue-like mechanical properties, improved cell adhesion and protein binding, and the ability to incorporate bioactive molecules and degradable components that support dynamic cell–matrix interactions.

The advent of 3D bioprinting technologies has further expanded the possibilities for creating biomimetic vascular models. Bioprinting enables the fabrication of complex, multilayered vascular structures with precise control over geometry and cellular composition.[20–22] This approach holds great promise for recreating patient-specific vascular anatomies and studying thrombosis in the context of personalized medicine. The ability to precisely position multiple cell types and materials in three-dimensional space allows for the creation of more sophisticated models that better reflect the complexity of native blood vessels.

This review aims to provide a comprehensive overview of the evolving landscape of *in vitro* thrombosis models, focusing on the transition from traditional PDMS-based microfluidic devices to advanced hydrogel-based systems and 3D bioprinted vascular constructs. We will discuss the strengths and limitations of each approach, highlighting their contributions to our understanding of thrombosis mechanisms. Furthermore, we will explore the integration of these technologies with perfusion systems to create more physiologically relevant "vessel-on-a-chip" platforms for thrombosis research. By examining the current state of the art and identifying remaining challenges, this review seeks to provide insights into future directions for developing increasingly sophisticated and clinically relevant *in vitro* thrombosis models.

Lining Arnold Ju

Prof Ju is a Snow Fellow, Australian Academy of Science John Booker Medalist and GT-40Under40. He received PhD at Georgia Institute of Technology and Emory University. In early 2020, Dr Ju joined the University of Sydney's new School of Biomedical Engineering and started up the Mechanobiology and Biomechanics Laboratory. Prof Ju's vision is to build novel platforms that integrate advanced biomanufacturing, high-throughput biomechanical manipulation, and artificial intelligence for mechanobiology. His track record spans developing, characterising, and evaluating innovations of 3D organ-on-chips, bioelectronic sensors, generative AI in biofabrication, and point-of-care microtechnologies.

2. Current understanding of vascular thrombosis and existing research gaps

2.1 Complexity of the vascular system

The native vasculature system is a complex network that integrates biochemical and biophysical signals *via* systemic transport of blood, nutrients, and inflammatory and pathogenic moieties across the endothelium to surrounding ECM matrix or from tissues into the bloodstream.[23] Blood vessels are organized in a 3D space in a hierarchical branching network with a range of dimensions spanning from a diameter of about 1 cm for large vessels like the aorta and vena cava to only 5 μm in capillaries.[24,25] Table 1 summarizes the key differences between arteries, veins, and capillaries in terms of their structural composition, dimensions, physiological functions, and associated pathological conditions.

The vascular wall is organized in three layers known as tunica intima, tunica media, and tunica adventitia intercalated by elastic membranes. The innermost layer is composed of endothelial basement membrane and proteoglycan-rich glycocalyx with a monolayer of endothelial cells lining the lumen of all blood vessels.[32] The middle layer, tunica media, consists of circumferentially aligned contractile vascular smooth muscle cells (vSMCs) and ECM that are both passive and active load bearings components functioning as expansion and contraction during cardiac cycle. The outermost adventitia layer is composed of fibroblasts and loose fibrillar collagens, which can contribute to compressibility of vessel wall and keep the vascular structure intact by remodelling.[33–35] Pericytes wrap around endothelial cells in capillaries, precapillary arterioles and postcapillary venules that do not contain vSMCs, functioning as macrophages as well as smooth muscle cells and contributing to regulation of blood flow, angiogenesis, maintenance of vascular permeability and immunomodulation in microvasculature[7,36] (Fig. 2A).

Table 1 Blood vessels composing of arteries, veins and capillaries, which differ in structural composition, dimension, physiological function and its pathological conditions. Abbreviations: EC, endothelial cells; VSMC, vascular smooth muscle cells; DVT, deep vein thrombosis; NA, non-accessed

	Artery	Vein	Capillary
Diameter	0.02–10 mm (ref. 26)	0.03–12.5 mm (ref. 26)	5–20 μm (ref. 26)
Vascular cells	EC, VSMC and fibroblast	EC, VSMC and fibroblast	EC, pericyte
EC phenotype	Long and narrow[27]	Short and wide[27]	Thin and irregular[28]
Shear stress, pressure	10 to 70 dyn cm^{-1},[2,29] 90–100 mmHg	1 to 6 dyn cm^{-1},[2,29] 5–15 mmHg	10 to 20 dyn cm^{-2} (ref. 30)
Valves	Absent	Present	Absent
Physiological Function	Blood pressure control by elastic recoil in the large arteries and vascular resistance in arterioles[30]	Reservoir, temperature regulation, leukocyte emigration[30]	Gas and nutrient transport with underlying tissues[30]
Pathological conditions	Atherosclerosis, embolus, aneurisms[30]	Varicose veins, DVT, pulmonary embolism[30]	Diabetic retinopathy, neuropathy and nephropathy[31]

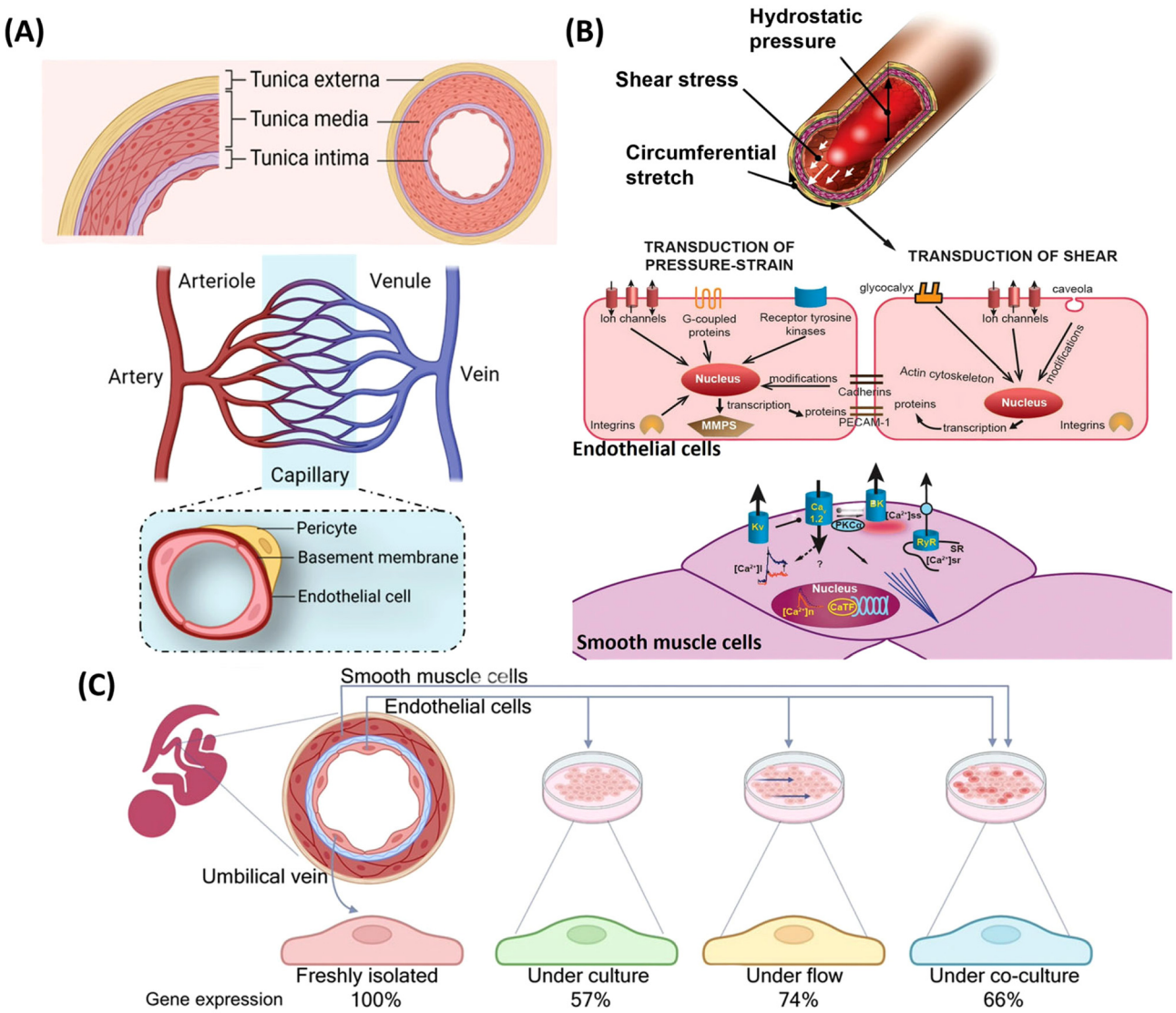

Fig. 2 (A) Schematics illustrating structural composition of blood vessels in a hierarchical network of vascular bed. Created with BioRender.com. (B) Graphical illustration of hemodynamic signals in vessels (hydrostatic pressure, shear stress, and circumferential stretch) that can be sensed by endothelial cells and adjacent smooth muscles cells to modulate vascular adaptation.[48] (C) Schematic representation comparing gene expression profiles of vascular cells *in vivo* and different *in vitro* conditions.[47]

The innermost endothelium is unique and functions as a dynamic organ where apical (luminal) surfaces of ECs are continuously in direct contact with blood circulation and their basolateral (abluminal) surfaces are residing on vascular matrix.[37] The flow of blood and pressure exerts a mechanical force (*i.e.*, transmural pressure, circumferential stress and tangential shear stress) that can potently modulate nearly all facets of vascular function by activating signalling pathways and modify gene expression patterns in the cells[38,39] (Fig. 2). Whilst fluid shear stress from blood flow mainly affects endothelial cells and their function, transmural and circumferential stress in the vessel wall arising mainly from local blood pressure regulate SMCs activities in tunica media and fibroblasts in adventitia.[40,41] Regulating vascular tone by the release of vasodilators or vasoconstrictors[42] and concomitant vascular remodelling are orchestrated by endothelial cells and vSMCs or pericytes[43] in response to intramural blood pressure and flow.[44] Different types of vascular cells communicate with each other to maintain healthy blood vessels that ensure the right balance between vessel integrity and permeability.[45,46] It is demonstrated that removal of HUVECs from umbilical cord of newborn babies could impact their inherent behaviour, function and gene expression (Fig. 2C),[47] highlighting the significance of dynamic haemodynamic forces and cellular crosstalk to be simulated in *in vitro* vascular model that could govern behaviour of endothelial cells and vascular tone *via* signalling feedback by cell mechanosensing.[38]

2.2 Virchow's triad and thrombosis

Within the complex vascular network described in the previous section, Virchow's triad emerges as a fundamental framework for understanding thrombosis pathophysiology. This triad comprises three key elements: endothelial cell injury, hemodynamic flow disturbance, and hypercoagulability. Each of these components is intricately linked to the structural and functional aspects of blood vessels, including the endothelial lining, smooth muscle cells, and surrounding extracellular matrix.[11]

The endothelial injury component of Virchow's triad is directly related to the integrity of the tunica intima, the innermost layer of blood vessels. Damage to this layer can expose the underlying basement membrane and trigger the coagulation cascade. Hemodynamic flow disturbances, the second component of the triad, are heavily influenced by the vessel geometry and the dynamic forces exerted by blood flow, as will be further explored in the following section on hemodynamic forces. These disturbances can occur in areas of complex vascular geometry, such as bifurcations or stenotic regions, leading to altered shear stress patterns that can activate endothelial cells and platelets. The third component, hypercoagulability, involves an increased tendency for blood to clot due to alterations in the balance of pro- and anti-coagulant factors, which can be influenced by both genetic and acquired factors. These three components are often interlinked and influence each other in thrombotic diseases, where endothelial damage can exacerbate flow abnormalities and hypercoagulability, forming a complex pathological network that promotes thrombosis.

While hemostasis represents a physiological response to vascular injury, forming a temporary hemostatic plug to stop bleeding, thrombosis refers to the pathologic formation of a thrombus (clot). This process is often associated with inherited or acquired risk factors driven by aging, genetics, lifestyles, and medical conditions of individual patients.[49] The interplay between these factors and the components of Virchow's triad contributes to the highly heterogeneous nature of thrombotic events among individuals.

Current diagnostic and surveillance strategies poorly capture the complex interplay among these three factors of Virchow's triad as focusing on just one gives an incomplete view of thrombosis. This limitation stems from the difficulty in simultaneously assessing endothelial function, blood flow dynamics, and coagulation status *in vivo*, particularly given the structural complexity and variability of the vascular system. Consequently, there is a growing recognition of the need for more sophisticated *in vitro* microfluidic models that can replicate the conditions described by Virchow's triad under controlled settings.

The development of microfluidic and vessel-on-a-chip models offers a unique opportunity to study the interplay of Virchow's triad components under precisely controlled conditions. These models can be designed to mimic specific vascular geometries, incorporate cultured endothelial cells, and allow for the manipulation of flow conditions and coagulation factors.[11,50,51] By bridging the gap between the structural complexity of the vascular system and the dynamic forces acting upon it, these models pave the way for a more nuanced understanding of thrombosis pathophysiology.

2.3 Hemodynamic forces in vasculature

Endothelial cells are normally in a quiescent state, but they are activated in response to chemical and mechanical stimuli such as inflammation or hydrodynamic stress to induce a prothrombotic state. In the native environment, ECs are continuously exposed to circulating blood and the force of luminal blood flow against vascular wall exerts a frictional force called wall shear stress (WSS) on the native endothelium, which is regarded as an essential mechanical cue for angiogenesis, cellular signalling, mass transport and vascular homeostasis (*i.e.*, a balance between pro- and anti-coagulant activity of blood and pro- and anti-inflammatory environment in tissues).[52–54] The flow patterns and hemodynamic forces are not uniform in real vascular system[55] in which shear stress is affected by complex vascular geometries; as such ECs, smooth muscle cells differentially respond through cellular mechanotransduction pathway (Fig. 2B). For example, unidirectional laminar flow found in healthy straight artery (10 to 70 dyn cm^{-2}) or venous system (1 to 6 dyn cm^{-2}) maintains vascular homeostasis and have atheroprotective effects by preventing plaque accumulation. The laminar flow promotes ECs to maintain anti-thrombotic, anti-proliferative and anti-inflammatory phenotypes through a biochemical response to the flow of blood

(Fig. 3A).[29,46,56] The healthy endothelium suppress platelets/blood cells adhesion and does not activate coagulation cascade by producing vasoprotective or thromboresistant molecules such as prostacyclin (PGI_2), nitric oxide (NO), and ecto-adenosine diphosphatase (ADPase).[57]

By contrast, turbulent and multidirectional flow or low oscillatory shear stress (<4 dyn cm^{-2})[13] created in stenotic/bifurcated/atherosclerotic plaque or mural thrombosis area leads to increased turnover of ECs, endothelial barrier dysfunction and procoagulant endothelial phenotypes that are prone to atherogenic or thrombogenic (Fig. 3A)[23,46,47,58] by increased expression of leukocyte adhesion molecules,[46] von Willebrand factor (VWF), tissue factor (TF), and enhanced thrombin generation.[29] A growing body of research also suggests the shear induced platelet activation, aggregation, and fibrin deposition mechanisms,[50,59–61] with platelet-rich white clot in arterial tree and fibrin-rich red clot in venous bed.[62,63]

It can be instrumental in observing the effect of hemodynamic force ranging from fluid shear, the tangential force derived from the friction of blood flow across the luminal cell surface, tensile stress due to deformation of the vessel wall by transvascular flow, and normal stress caused by the hydrodynamic pressure differential across the vessel wall (Fig. 3B).[52] By observing the behaviour of endothelial cells under different flow conditions, researchers can dissect the response of ECs to mechanical forces/inflammatory mediators, shear-induced thrombosis under physiological and pathological conditions, development of vascular pathologies such as atherosclerosis, thrombosis, in-stent restenosis as well as their clinical complications.[55]

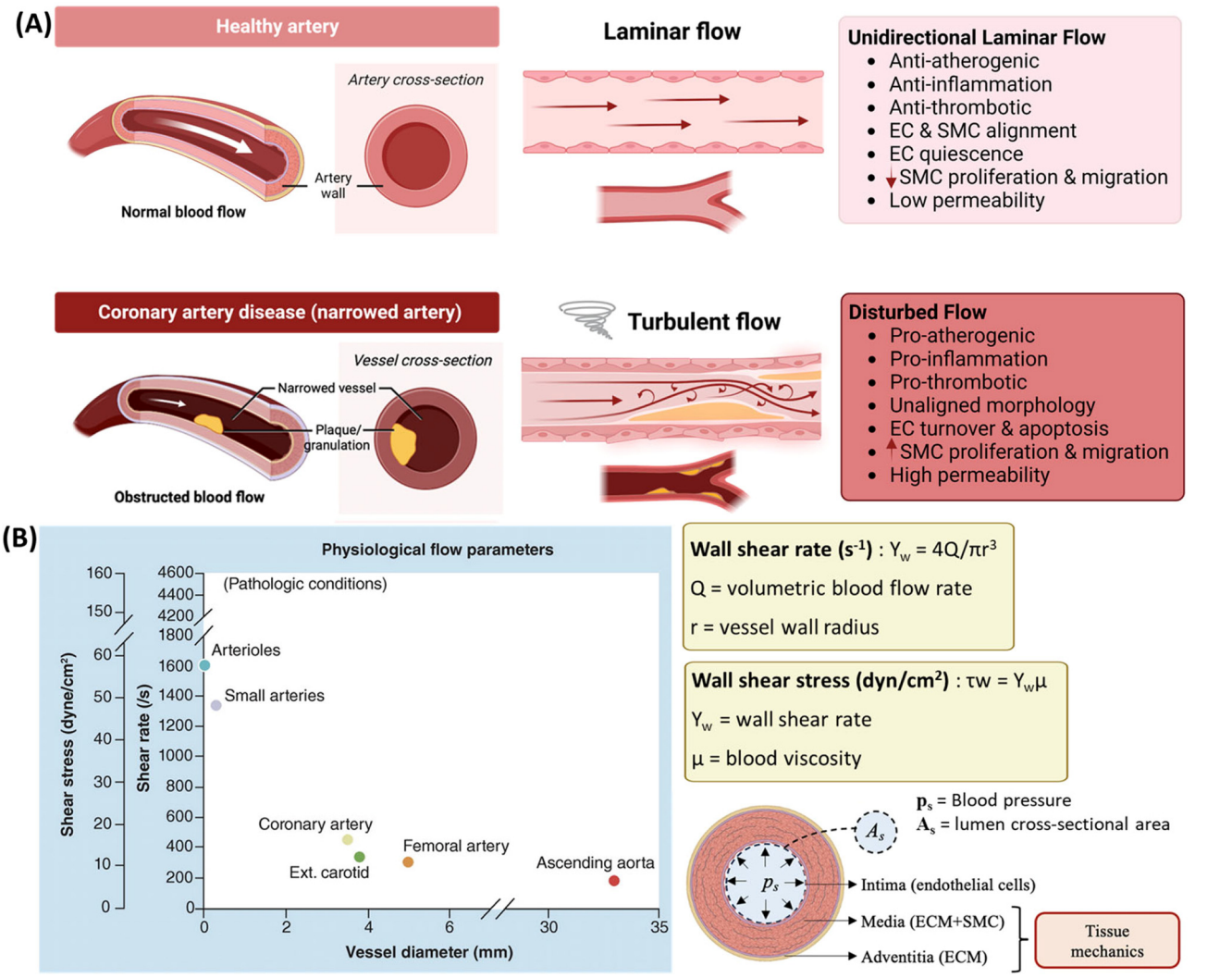

Fig. 3 (A) Laminar flow in healthy smooth vessel *versus* turbulent flow in stenosed atherosclerotic vessel. Laminar flow protects vessels from atherosclerotic plaque formation and thrombosis, whereas turbulent flow is susceptible to atherosclerosis and thrombus formation.[55,64] Figures created with BioRender.com. (B) Vessel wall shear rates and corresponding shear stresses of various vessels under normal physiological and pathological conditions.[42,65]

2.4 Mechanobiological effects of flow and shear on vascular cells

Continuous disturbed blood flow is responsible for endothelial-to-mesenchymal transition (EndMT) and endothelial-to-immune cell transition (EndIT), stimulating pathological angiogenesis or arteriogenesis such as progression of atherosclerosis with endothelial reprogramming into distinct cell types.[40,66–68] Apart from the external hemodynamic forces driven from blood flow, ECs are also continuously exposed to mechanical cues in the form of matrix stiffness[34] since basement membrane and surrounding vascular tissues are highly plastic and tend to become stiffer due to flow-mediated remodelling process[69] or other predisposing factors (*i.e.*, hypercholesteremia, hypertension, hyperglycaemia).[70] Focal adhesions serve as highly dynamic mechanotransducers of the ECM stiffness and Erk1/2 and eNOS signalling molecules mediated by focal adhesion kinase (FAK) are known to play key roles in vascular homeostasis in response to the mechanical cues from ECM, with the former regulating EC proliferation and the latter mediating vasodilator (NO) release.[13] Physiological ageing or pathological arteriosclerosis/atherosclerotic condition contribute to vascular stiffness arising from degenerative process of ECM (*i.e.*, elastin fibres degraded and replaced by more collagen fibres production, shifting the arterial wall toward a stiffer range).[71]

The ratio of collagen to elastin in the ECM determines the vascular tissue stiffness, which is characterized by Young's (elastic) modulus (Pa or N m^{-2})[32] and the Young's modulus of intact artery in human is reported to be 0.3–1.0 MPa for elastin, 100–1000 MPa for collagen and overall 1–5 MPa.[7,72] The mechanical property of intact blood vessel is known to be viscoelastic rather than elastic and its viscoelastic nature reduces dynamic stresses and strains in vessel wall.[73] The elastic modulus of native vessels has been reported by a wide range of values from 0.1–1.5 MPa,[39,74] which can increase up to ~3.8 MPa in atherosclerotic vessel.[75] At low blood pressures (<80 mmHg), the mechanical behaviour of artery is dominated by the elastic components which are less stiff. In the physiological range of pressure (80–120 mmHg), the load transits between the elastin and collagen fibres. With increasing pressure (>120 mmHg), the collagen and elastin fibres have become gradually stretched and they are dominated by the stiffer collagen fibres to adapt greater amount of circumferential load with a change in the diameter. The rigid collagen fibres also prevent the damage and/or rupture of blood vessels in response to high pressure.[72] As consequence of arterial stiffness, increased local arterial resistance leads to change in oscillatory shear stress and increased blood pressure/tensile stress,[76] which is followed by endothelial dysfunction with loss of ECs markers such as VE-cadherin, PECAM-1 [7] and compromised barrier integrity.[75,77]

There is a pressing need for an increased understanding of the mechanisms by which the structural and functional changes occur within the vascular wall in response to sustained increased blood pressure and shear stress, that defines overall vascular mechanics. A central question is how the hemodynamic forces and mechanical factors are sensed by the cells of the vessel wall and then translated into pathophysiologically relevant changes in terms of vascular cells morphology, senescence, proliferation, differentiation and inflammation, vascular tone, and ECM remodelling, that could be susceptible to vascular pathologies and promotion of thrombosis.

2.5 Research gaps and challenges

The majority of current thrombosis research has relied on blood tests, including protein fragments found in blood clots (*i.e.*, D-dimer)[78] and platelet function analyses[79,80] to rule out clotting conditions and forecast thrombotic risk. Most of these tests yield quantitative results in a laboratory without giving due consideration to the crucial role of vessel wall characteristics and dynamic blood flow patterns, in which false negative and false positive findings are inevitable.[81,82] Current practices are generally based on empirical antithrombotic therapy,[83] highlighting the need for personalized diagnostic testing options based on individualized Virchow's triad for thrombotic risk stratification and long-term monitoring.

Several research gaps and challenges remain in the field of thrombosis research:

1. *Multicellular interactions*: the complex interplay between endothelial cells, platelets, leukocytes, and other vascular cells in thrombosis is not fully understood. Current *in vitro* models often focus on individual cell types, limiting our ability to study these interactions in a physiologically relevant context.

2. *Biomechanical factors*: the influence of mechanical forces, including fluid shear stress and vessel wall stiffness, on thrombosis needs further investigation. Most *in vitro* models fail to accurately recapitulate the dynamic mechanical environment of blood vessels.

3. *Patient-specific variability*: individual differences in thrombotic risk and response to antithrombotic therapies are not well-captured by current models. There is a need for personalized approaches to study thrombosis and develop tailored treatments.

4. *Tissue-specific thrombosis*: different vascular beds (*e.g.*, arterial *vs.* venous, organ-specific vasculature) exhibit distinct thrombotic behaviors. Models that can accurately represent these tissue-specific differences are lacking. Current technologies and biomaterials for 3D EC culturing have made significant progress in fulfilling the hemodynamic part of Virchow's triad. However, there is still a need to better understand how cultured ECs respond to injury stimuli in different models and materials, addressing another crucial part of Virchow's triad.

5. *Chronic conditions*: the long-term effects of chronic diseases (*e.g.*, diabetes, hypertension) on vascular health and thrombotic risk are challenging to study *in vitro*. Developing models that can simulate these chronic conditions remains a significant challenge.

6. *Drug testing and development*: while animal models are widely used for drug screening, they often fail to predict human responses accurately. There is a need for more predictive *in vitro* models for antithrombotic drug development and testing.

7. *Thrombosis resolution*: the processes involved in thrombus resolution and vessel recanalization are not well-under-

stood. Models that can capture the entire lifecycle of a thrombus, from formation to resolution, are needed.

Overall, the traditional 2D microfluidic chip models are limited in their ability to mimic key physiological parameters like 3D construct, viscoelasticity, complex cell–cell crosstalk, cell–niche interactions, and vascular permeability found in native microvascular environment. Although animal models capture these features, there are limited animal models, unsuitability for real-time visualisation of disease progression, ethical concerns, and possible species differences between human and animals in translating disease characteristics or drug responses.[84] To address these research gaps, there is a growing need for more sophisticated *in vitro* models that can better recapitulate the complexities of the vascular environment. The integration of advanced biomaterials, microfluidic technologies, and tissue engineering approaches offers promising avenues for creating more physiologically relevant thrombosis models. Various vascular models with their capabilities to simulate complex blood vessels are summarized in Fig. 4.

3. Microfluidic models: their strengths and areas for improvement

The biological effects of flow and shear stress on endothelial cells under physiological and pathological hemodynamic conditions have become the focus of vascular biology and thrombosis research.[61,85,86] Given the optics limitation in deep vasculature tissue in *in vivo* models, studies of EC responses to external shear stress and clotting mechanisms have been revolutionized by microfluidic and on-chip technologies. These platforms offer unprecedented control over the microenvironment, allowing researchers to dissect complex biological processes with high precision.

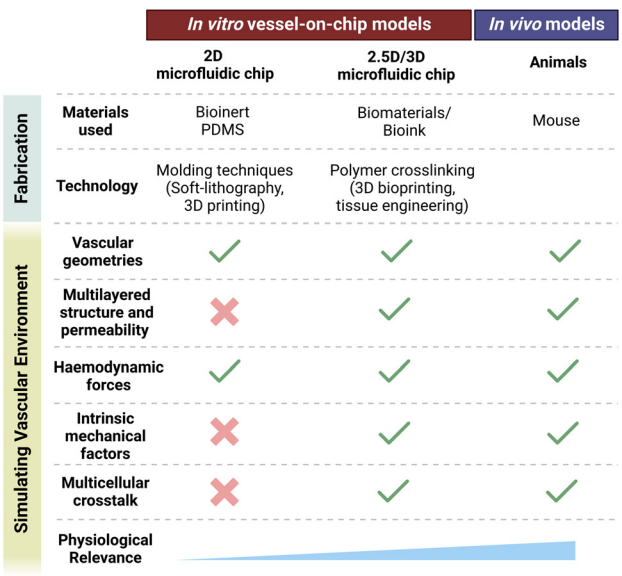

Fig. 4 In vitro vessel-on-a-chip models to recapitulate complexities of blood vessels that found in *in vivo* animal model.

Microfluidic chips generally contain a series of interconnected microchannels, inlet and outlet ports which are equipped with a pump, enabling real-time visualization and investigation of cellular dynamics and fluid flow through the microchannels under precisely controlled flow patterns and shear stress. Due to the miniaturized nature of the platform, only a low amount of cells and reagents are required, which is cost-efficient.[87] This efficiency, coupled with the ability to parallelize experiments, makes microfluidic devices particularly attractive for high-throughput screening applications in thrombosis research and it has a competitive edge over animal experimentation.

A range of microfluidic chips have been devised to mimic vascular geometries[88,89] incorporate haemodynamic parameters, and investigate thrombotic mechanism.[50,51,90,91] Looking at their timeline, innovations of microfluidic chip have relied on other contemporary technologies such as soft lithography,[50,92] patterning paper,[93,94] 3D printing,[51,95] and other emerging fabrication methods (Fig. 5).

One of the key strengths of microfluidic models in thrombosis research is their ability to recreate the complex flow conditions found in different vascular beds. This is particularly important given that different regions of the vasculature exhibit distinct clot compositions and thrombotic behaviours. For instance, arterial thrombi are typically platelet-rich (white clots), forming under high shear conditions, while venous thrombi are more fibrin-rich (red clots), developing in areas of low flow and stasis. By allowing the creation of tissue-specific vascular geometries and flow conditions, microfluidic models enable researchers to study these differences in a controlled environment.

Researchers have leveraged these capabilities to perfuse whole blood samples through a range of vessel-on-a-chip designs, testing the efficacy of certain drugs in microvascular occlusion and thrombosis.[98–101] With small quantities of blood running through specially designed shear-specific microfluidic devices that simulate stenosis or atherosclerotic plaque,[50,100,102] blood clots are prone to occur in the high shear zone area of injured endothelium (Fig. 6A). By simulating patient' vascular geometries based on clinical imaging (*e.g.*, CT/MRI scan) to fabricate personalised vein chips, researchers can validate the potential of blood clot formation in specific region.[51] This approach not only indicates the tendency of blood clot formation, alerting the requirement of prophylaxis, but also allows for detailed analysis of clot composition and structure.

Upon testing clotting time with respect to drug screening (*e.g.*, anti-platelet drug Abciximab) using patients' own blood perfusion, controlled antiplatelet patients can readily monitor efficacy of their antithrombotic therapies and individual's clotting risk factor in both hospital or home care setting.[100] The analysis of clot composition formed in these devices can also differentiate between fibrin-rich and platelet-rich clots,[50] providing valuable information for clinicians in prescribing appropriate antithrombotic therapies. For instance, this information can guide the choice between anti-platelet drugs (*e.g.*,

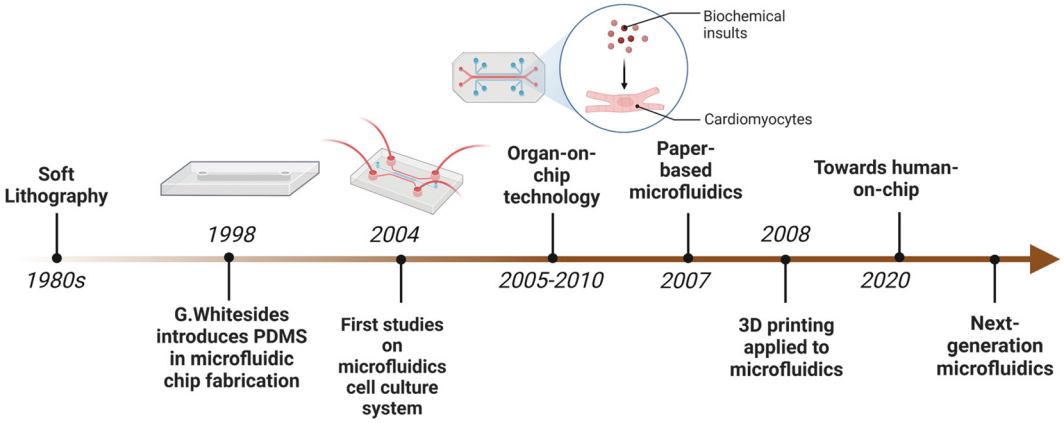

Fig. 5 Timeline of microfluidic chip models generated through various platform.[96,97] Figure created with BioRender.com.

aspirin, clopidogrel)[103] or anticoagulants (*e.g.*, warfarin, heparin),[104] potentially alleviating the side effects associated with empirical therapy. Furthermore, identifying the physical characteristics of blood clots can help assess the risk of unstable clots potentially migrating to distant smaller vessels, such as in thromboembolism, which is crucial for patient prognosis and determining the need for follow-up visits.

As such, microfluidic chips have significant potential for use as personalized diagnostic devices to detect blood clotting tendency, screen anti-thrombotic drugs, and predict the fate of thrombus formation (Fig. 6B). This potential for personalization represents a major advance in thrombosis research and management, offering the possibility of tailored treatment strategies based on individual patient characteristics.

3.1 PDMS-based vessel-on-a-chip

Polydimethylsiloxane (PDMS) has been the material of choice in the microfluidic field for many years, owing to its excellent moldability, optical transparency, and cost-effectiveness.[105] These properties have made PDMS an ideal material for creating vessel-on-a-chip models, allowing for easy fabrication of complex channel geometries and real-time visualization of cellular and fluid dynamics.

A wide range of PDMS-based vessel-on-chips have been developed to mimic diseased vascular geometries reminiscent of atherosclerosis, stenosis, and aneurysms in varying degrees of severity.[88,89,102,106] These models have proven invaluable in simulating damaged endothelium and prothrombotic conditions using various stimuli such as LPS endotoxin,[107] TNF-α,[108] PMA[50,51] and laser irradiation,[109] to investigate thrombotic mechanism by incorporating haemodynamic parameters.[50,51,90,91,106] (Fig. 7). The Virchow's triad-induced thrombosis has been extensively studied *in vitro* using these traditional PDMS-based microtechnologies, which were first introduced in 1998. To date, these compact and cost-efficient microfluidic chips have been regarded as the most suitable tools to model normal (atheroresistant) or diseased (atheroprone) vascular conditions for high-throughput, rapid, and scalable blood clot testing.

One of the key advantages of PDMS-based models is their ability to recreate the dynamic flow conditions found in blood vessels. Considering that native blood vessels are subjected to shear forces from blood flow and that soluble factors in the bloodstream are accessed from the apical (luminal) sides of endothelial cells,[86] it is highly relevant to implement dynamic cell culture systems using PDMS-based microfluidic channels. These systems provide a monolayer of polarized endothelial cells with directional cell alignment and allow for the study of pathological thrombus formation in response to flow shear stress.[12,50,51,110]

However, despite these advantages, PDMS-based models have several limitations that have driven the field towards more advanced materials and designs. One significant drawback is that the basolateral membranes of endothelial cells in PDMS channels rest on an unphysiologically rigid artificial substrate. It has been observed that endothelial cell morphology, intracellular organization, and barrier integrity are drastically altered according to substrate stiffness, as the basal sides of ECs possess integrin mechanosensors.[13,77,111–113] This mismatch in mechanical properties between PDMS and native vessel tissue can lead to cellular behaviors that may not accurately reflect *in vivo* conditions.

Another limitation of PDMS is its high hydrophobicity and bioinert characteristics. To address these issues, various surface modifications have been employed.[114] These include plasma treatment to improve hydrophilicity[115,116] that promote adsorption of ECM molecules and a thin layer coating with ECM proteins such as collagen,[109] gelatin,[117] laminin,[118] fibronectin[50,51] and other polymers like polyethylene glycol (PEG), poly-L-lysine,[119] and polydopamine[120] to enhance biological activity and cell attachment. However, despite these efforts, the surface properties of modified PDMS still do not fully satisfy the biocomplexity of the native ECM environment.

Furthermore, the 2D culture within PDMS-based models limits their ability to recapitulate the full complexity of the 3D vascular microenvironment. While the native endothelium can be viewed as an essentially 2D monolayer in a planar format, the surrounding matrix and supporting cells *in vivo* exist in a

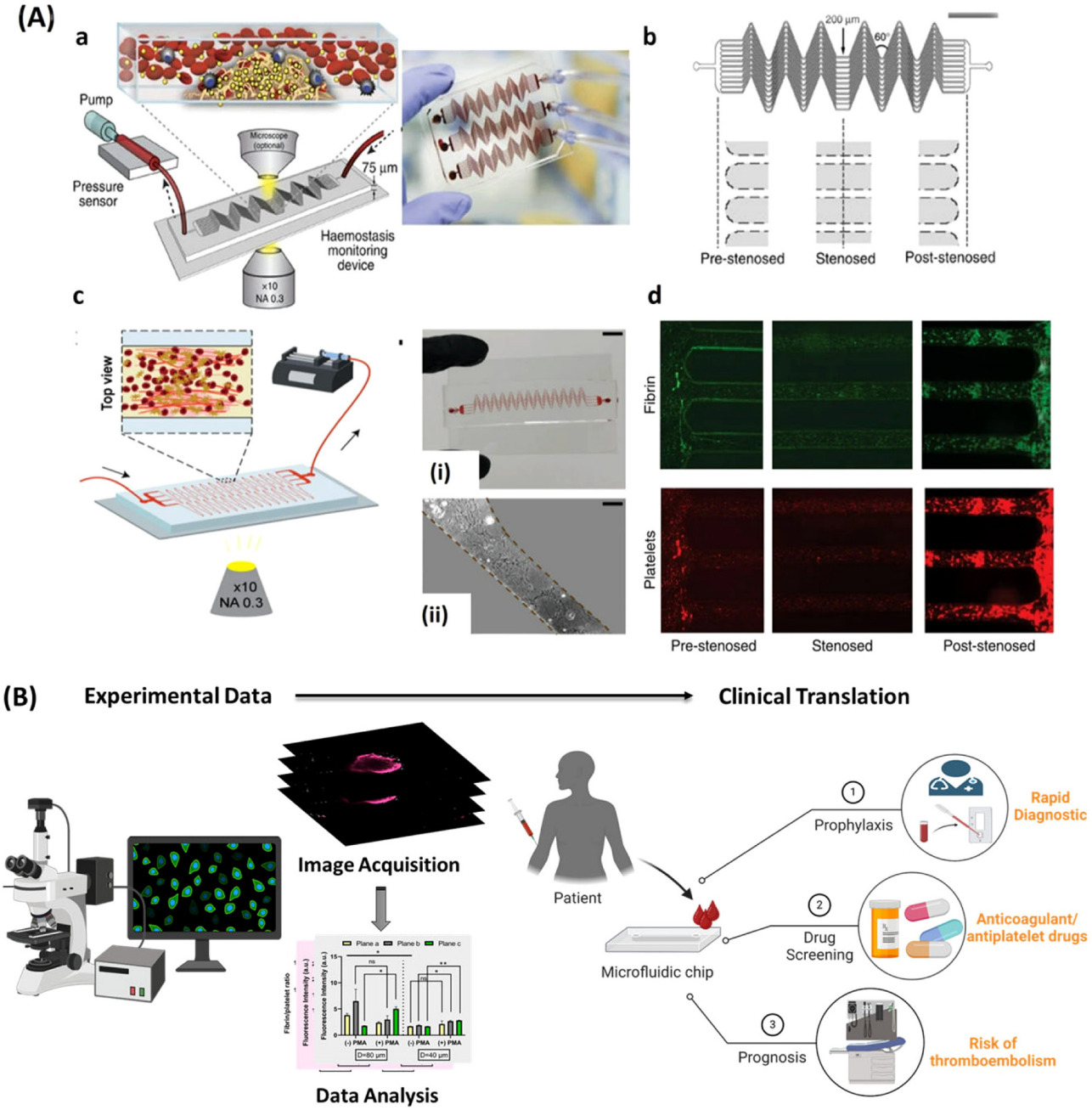

Fig. 6 (A) Microfluidic devices for haemostasis and thrombosis research. (a) Schematic of the haemostasis monitor devices and blood perfusion. Human whole blood is pushed or pulled by a syringe pump that connects to the device *via* tubing to determine micro-clotting time. (b) Diagram of the device with line drawings illustrating the design of the accelerating (pre-stenosed), uniform width (stenosed) and decelerating (post-stenosed) regions of the microchannels. The central stenosed region contains 12 parallel lanes of 200 μm-wide and 75 μm-high channels that repeatedly turn 60° a few times in each channel (scale: 500 μm).[100] (c) Schematic of the microfluidic device mounted on a microscope and connected to a pump that pulls blood to determine clotting time, (c-i) Photograph of the microfluidic device (scale: 10 mm), (c-ii) Representative image of collagen coating a section of the microdevice (scale: 100 μm).[101] (d) Fluorescence microscopy of fibrin (green) and platelets (red) in monitoring of thrombus formation in pre-stenosed, stenosed, and post-stenosed regions after perfusing blood through the device, containing heparin (0.25 IU ml^{-1}) for 20 min (scale: 500 μm).[100] (B) Translating experimental data to clinical applications in bench-to-bed side thrombosis management. Figures created with BioRender.com.

3D configuration. This limitation becomes particularly apparent when trying to incorporate other integral microvascular cell types such as smooth muscle cells and pericytes into PDMS-based models.

In summary, the traditional PDMS microfluidic device in 2D plane which lack viscoelasticity, mass transfer and anatomies of native vessel cannot meet the demands of dynamic reciprocity between cells and ECM in 3D microvascular struc-

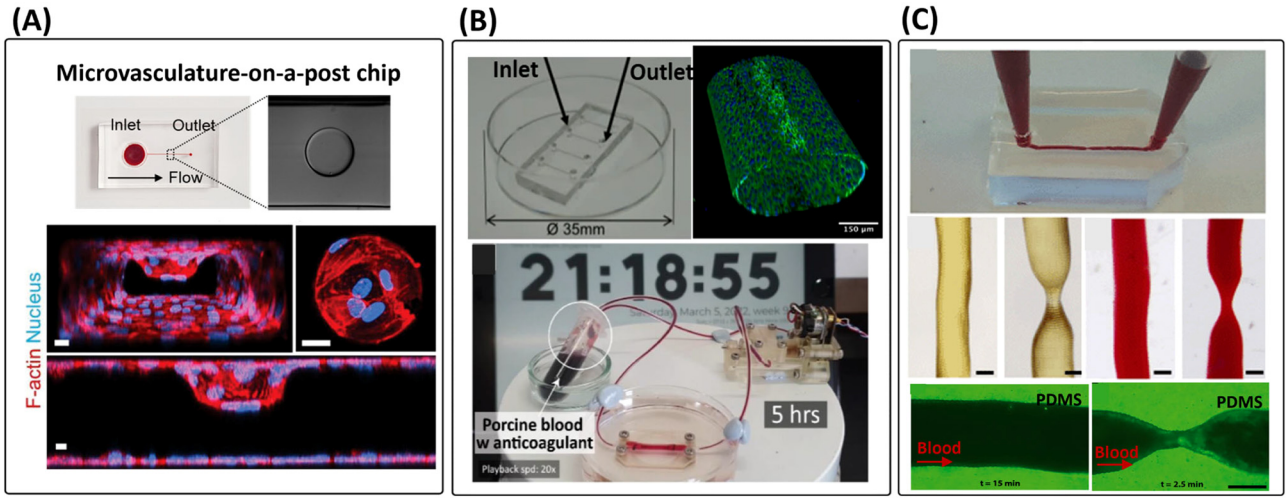

Fig. 7 PDMS-based vessel on chip for thrombosis research. (A) Microvasculature-on-a-post chip, simulating stenotic vessel.[50] (B) Multi-circular channels fabricated by embedding needles in PDMS and perfusion of porcine blood.[121] (C) 3D printing based PDMS chip analogues to healthy and stenotic vessel and thrombosis occurred at the apex of stenosis on blood perfusion. Scale bar = 200 μm.

ture *in vivo*. While PDMS-based microfluidic devices have made significant contributions to our understanding of thrombosis, particularly in terms of flow dynamics and basic endothelial cell responses, they fall short in modelling the intrinsic biophysical and biochemical properties of the *in vivo* vessel wall. The rigid nature of PDMS, its limited permeability, and the challenges in creating truly 3D architectures have led researchers to explore alternative materials and approaches, particularly hydrogel-based systems.

3.2 Hydrogel-based vessel-on-a-chip

To address the limitations of PDMS-based models, hydrogel-based microfluidic devices have gained prominence in recent years.[13–15] These systems offer the potential to produce more biologically relevant chips that better mimic the native vascular microenvironment. Hydrogels are crosslinked networks of nanofibers that allow large water content to be entrapped within their 3D networks. Through the design of a 3D architecture with a porous nature and fibrillar structure, scaffolds formed from hydrogels offer excellent support for cell attachment as they can imitate the ECM while transporting soluble components such as cytokines, growth factors, complement, and coagulation factors across the matrices.[32]

One of the key advantages of hydrogel-based systems is their tunable mechanical properties. The properties of hydrogels can be modified by varying polymer or crosslinker concentrations,[74,122] allowing researchers to create matrices with stiffness values that more closely match those of native blood vessel walls. This is crucial for accurate modeling of cellular mechanotransduction and behavior, as cells are known to respond differently to substrates of varying stiffness.

Furthermore, hydrogels can be functionalized with bioactive ligands,[123–127] serving as a source of both mechanical and biological cues. This property to incorporate specific signaling molecules into the matrix allows for more sophisticated control over the cellular microenvironment, enabling researchers to study the effects of various biochemical factors on thrombosis in a more physiologically relevant context.

The combination of microfluidics and hydrogels offers several advantages over traditional PDMS-based systems:

1. *Continuous perfusion*: hydrogel-based microfluidic devices allow for continuous perfusion of nutrients, soluble chemical and biological molecules, and the withdrawal of waste products.[128,129]

2. *Dynamic hemodynamic conditions*: these systems can more accurately recreate the flow conditions found in native blood vessels, including pulsatile flow and variable shear stress.

3. *3D cell culture*: hydrogels enable the encapsulation of cells within the matrix, allowing for more physiologically relevant cell–cell and cell–matrix interactions.

4. *Improved mass transfer*: the porous nature of hydrogels allows for better diffusion of nutrients and waste products, more closely mimicking the transport processes in native tissues.

5. *Tissue-specific modeling*: by tuning the hydrogel composition and mechanical properties, researchers can create models that more accurately represent different vascular beds and pathological conditions.

These features make hydrogel-based systems particularly well-suited for studying the complex interplay between endothelial cells, blood components, and the surrounding matrix in thrombosis.

There are two main approaches to obtaining hydrogel-based perfusable vascular networks: (1) bottom-up bioengineering: this approach involves vasculogenesis and angiogenesis using vascular units as building blocks.[130–134] While this method can lead to more organically formed vessels, it often results in unpredictable new vessel formation (*i.e.*, size,

geometry, and sprouting length) with uncontrollable flow patterns. (2) Top-down fabrication: this method involves pre-designing and pre-fabricating the desired architecture of the vascular bed before introducing endothelial cells.[133,135,136] The top-down approach gives rise to more precise vascular networks with well-defined and controlled flow patterns, making it more suitable for systematic investigation and practical applications of microfluidic vessel-on-a-chip models in thrombotic research.

Recently, numerous hydrogel constructs with hollow channels equipped with microfluidic devices have been developed *via* the top-down approach to provide biomimetic vessel-on-chips.[15,19,137] These can be established through a range of strategies:

1. *Molding and bonding*: this involves initial casting of hydrogels in master molds and then bonding the two hydrogel compartments *via* various crosslinking methods[15,18,19,137] (Fig. 8A).

2. *Template-based techniques*: these methods use sacrificial materials such needle,[134,138] glass pipette[17,134,135,139,140] stainless stee wire,[141] or encapsulation of gelatin meshes[14,142] or alginate[143] embedded in the hydrogel construct. The sacrificial material is then removed to create the channel (Fig. 8B).

3. *Advanced fabrication methods*: techniques such as 3D printing, photopatterning, and laser-based degradation have also been employed to create precise channel geometries within hydrogels.[144]

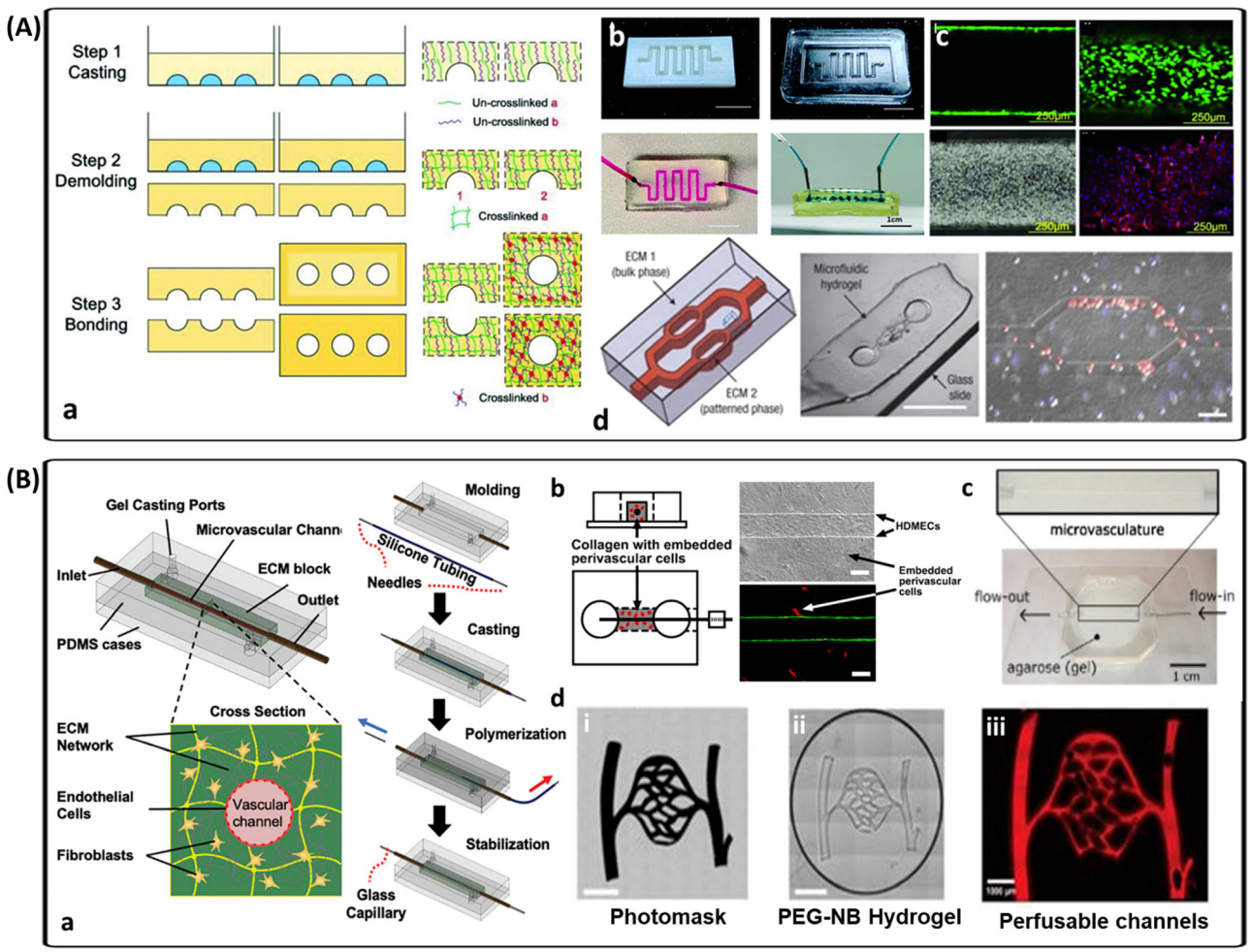

Fig. 8 Pre-patterned hydrogel-based microfluidic vascular chip fabricated by various methods. (A) Molding & bonding technique. (a) Schematics illustrating experimental steps involving casting, demolding and bonding to fabricate hollow vascular structure,[15] (b) pictures of hydrogel-based microfluidic systems including 3D printed resin mold, PDMS stamp, hydrogel chips with dye perfusion,[137] (c) optical and confocal images of endothelialised channels,[15] (d) diagram of a hydrogel construct with a microfluidically patterned phase and a bulk hydrogel phase, an image (middle) of the corresponding microfluidic hydrogel (taken with a stereoscope) (scale bar = 5 mm), fluorescence image overlay showing fibroblasts (blue) in the hydrogel bulk phase and HUVECs (red) in patterned collagen (scale bar = 100 μm).[145] (B) Template-based technique. (a) Schematics illustrating fabrication of vascular channel using a needle as template in a hydrogel block, (b) diagram and microscopic images (phase contrast (top) and corresponding fluorescent image (bottom)) showing vascular channel lined by HDMECs (human dermal microvascular endothelial cells (green)) and pericytes (red) embedded within the collagen matrix (scale bars = 100 μm),[139] (c) photograph of 3D microvasculature in agarose gel,[138] (d) brightfield images of (i) transparent photomask film, (ii) photopatterned hydrogel using the photomask as template (scale bar = 1 mm) and (iii) fluorescent image of the channels in the hydrogel perfused with dextran (red).[146]

These fabrication methods define the resolution (*i.e.*, dimension of microchannels inside the hydrogel), allowing for the creation of vessels with diameters ranging from capillary-scale (5–10 μm) to larger vessels (500–1000 μm). After channel formation, it is possible to seed endothelial cells in the pre-formed microfluidic channels, allowing them to populate the biomimetic lumen surface as a monolayer on the 2.5 D matrix. Meanwhile, the bulk hydrogel facilitates the encapsulation of other vascular cells, such as smooth muscle cells or pericytes, in the surrounding 3D matrix.

Several groundbreaking studies have demonstrated the potential of hydrogel-based vessel-on-a-chip models for thrombosis research: Zheng *et al*. pioneered establishment of collagen gel-based microfluidic vascular system with complex geometries and channel diameter as small as 40 μm to investigate onset and progression of microvascular thrombosis.[18] By varying a number of parameters in the microvascular gel system such as geometry, diameter, flow and blood components, VWF strands primarily secreted from endothelium unfold and form bundles and webs which are competent enough to bind platelets, leucocytes and erythrocytes, obstructing blood flow (Fig. 9A). Lam group also devised a perfusable, endothelialised microvascular-on-a-chip with tunable stiffness (5–50 kPa) and ∼20 μm channel using agarose–gelatin interpenetrating polymer network (IPN) gel to enable mechanistic insight into endothelial barrier dysfunction associated with haematological disease (Fig. 9B).[19] Sophisticated technologies like combined soft lithography and multiphoton ablation is also possible to fabricate capillary scale vessels (5–10 μm diameter) in collagen hydrogel and demonstrated microvascular obstruction mechanism in haematologic disease with malaria infected RBC sequestration and aggregation (Fig. 9C).[147]

These hydrogel-based models offer several advantages for studying vascular permeability and thrombosis:

1. *Barrier function*: the endothelial cell layer in these models forms a semi-permeable barrier, allowing for the transportation of small molecules such as water, ions, and nutrients between the bloodstream and surrounding tissues.[148] This capability, known as vessel permeability, is a key parameter in microvascular function and downstream signaling pathways.

2. *Vascular pathology modeling*: hydrogel-based models can reproduce vascular permeability changes and reactivity to inflammatory stimuli observed in various pathological processes. The implications involve atherosclerosis,[149,150] sickle cell disease,[19] diabetes,[151,152] certain infectious diseases caused by malaria,[153,154] COVID-19,[155] or bacterial lipopolysaccharide,[156] and cancer.[19,157]

3. *Endothelial induced inflammatory response*: these models allow for the study of endothelial barrier disruption caused by pro-inflammatory cytokines such as interferon-gamma (IFN-γ), tumor necrosis factor-alpha (TNF-α),[158] vascular endothelial growth factor (VEGF), interleukin-6, interleukin-1β, serotonin, bradykinin, substance P, histamine and thrombin.[37,41] This disruption leads to enhanced vascular permeability, extravasation of fluid and small solutes/macromolecules, and loss of microcirculatory flow.[159]

4. *Thrombosis mechanisms*: the dysfunctional endothelial cell surfaces in these models express adhesion molecules such as P-selectin, E-selectin, ICAM-1, and VCAM-1, which facilitate leukocyte rolling, adhesion, and diapedesis.[125,160,161] This process can trigger the coagulation cascade through VWF and neutrophil-derived tissue factor (TF)-rich neutrophil extracellular traps (NETs) formation (Fig. 10).[155,162]

In conclusion, hydrogel-based vessel-on-a-chip models represent a significant advancement in thrombosis research. By providing a more physiologically and pathophysiologically relevant 3D environment, tunable mechanical properties, and the ability to incorporate multiple cell types, these models offer unprecedented opportunities to study the complex interactions between endothelial cells, blood components, and the surrounding matrix in thrombosis. As these technologies continue to evolve, they hold great promise for unraveling the idiopathic mechanisms involved in various thrombotic disorders, including arterial and venous thrombosis, cancer-associated thrombosis (CAT), disseminated intravascular coagulation (DIC), and thrombotic thrombocytopenic purpura (TTP).

3.3 Material consideration for hydrogel-based vascular model

Hydrogel's tunable mechanical properties, porous in nature can truly mimic blood vessel's viscoelasticity and permeability, but hydrogel materials has some challenges regarding structural integrity of hollow vascular channels. Although swelling capacity is a crucial characteristics of hydrogels to display ability of fluid uptake to maintain a moist environment for tissue regeneration like wound dressing,[163,164] non-swelling or swelling-resistant hydrogel material is a favourable factor to consider in constructing patent vascular model with desired negative resolution, that enables retaining original structure and optimal mechanical performance in physiological aqueous environments.[165] Otherwise, swelling of hydrogels induce volume expansion of the artificial vascular tissue model, leading to reduction of internal vessel diameter with compromised integrity, stability, and functionalities. The swelling capability of hydrogel is not desirable in *in vitro* vascular model for thrombosis study that demands fabrication of patent lumen for dynamic flow analysis. To construct stable and functional *in vitro* vascular model throughout thrombosis investigation, hydrogel materials can be optimised to become resistance to swelling and more rigid but still in physiological range. Generally, the swelling capacity of hydrogel matrices can be suppressed by controlling pore size of the polymer network and polymer–water interactions such as increasing network crosslinking density,[166–169] incorporating hydrophobic segments,[170,171] diminishing ionic groups of polymers,[172] introducing brush polymer with multiple secondary side chains which exhibits steric constricts[173] or multiarmed polymer precursors.[174–176] Through UV crosslinked di-acrylated Pluronic F127 (PF127), Shen *et al.* fabricated autoclavable, non-swelling hydrogel-based microfluidic chips with outstanding mechanical and morphological fidelity in PBS at 37 °C and successful seeding of HUVECs endowed it with a functional vessel-on-a-chip model.[137] Various hydrogel materials are formulated to recapitulate native vascular stiffness as summarised in Table 2.

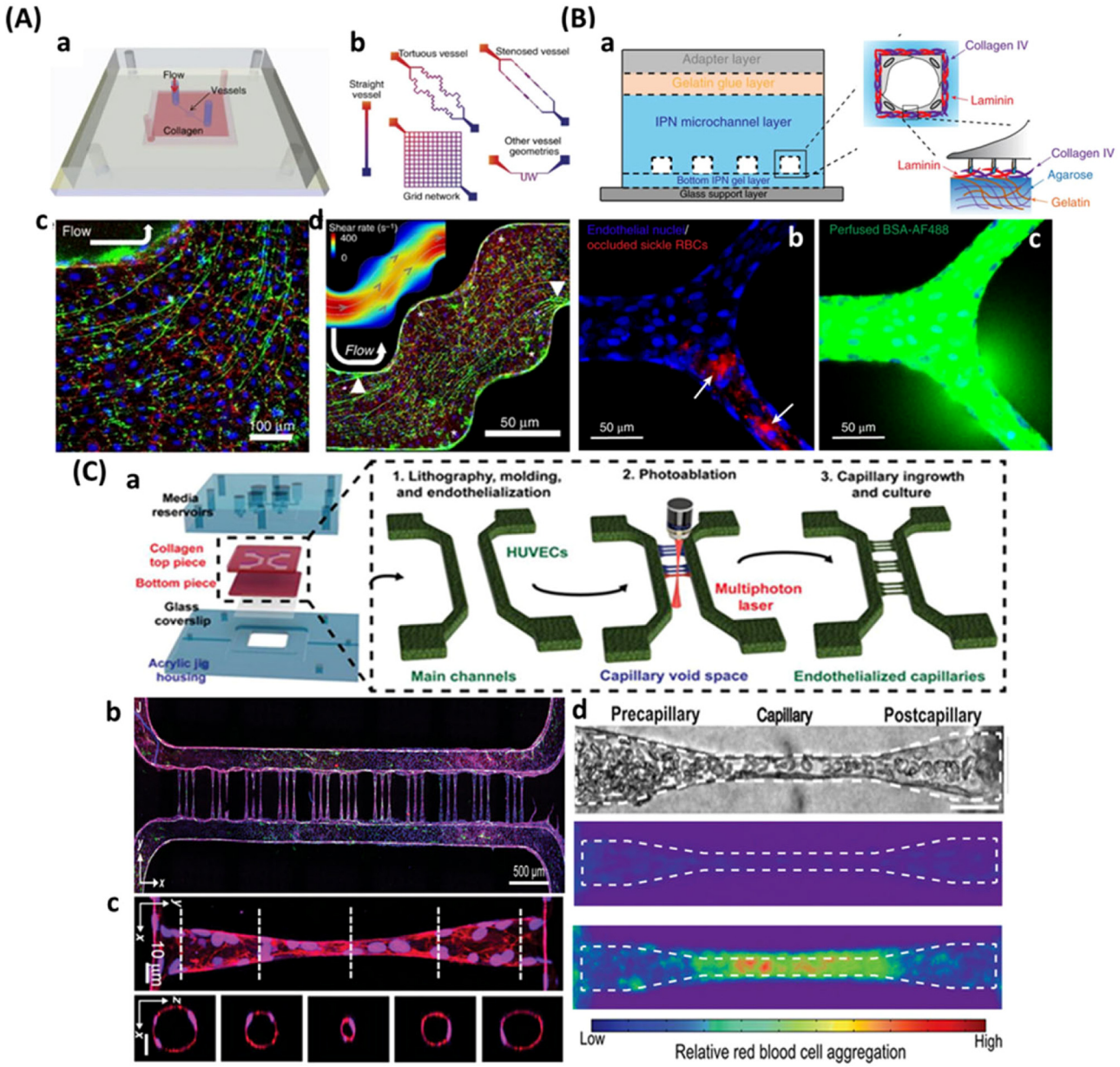

Fig. 9 3D hydrogel vascular models to investigate blood clotting mechanism. (A) (a) Schematic of a microfluidic microvascular system in collagen gel, (b) microvessel geometries (straight vessel, grid network, tortuous vessels, stenosed vessels and geometries using fonts or symbols). (c) VWF strands follow turns and direction of vessel wall in a 500 μm diameter vessel. (d) VWF strands remain bound to the vessel wall in a tortuous vessel with a diameter of 500 μm (arrowheads: individual VWF strands self-associated into thicker strands in regions of high shear stress; asterisks: regions of low shear stress lack VWF strands; green: VWF, blue: nuclei). The inset at the corner shows the COMSOL simulation of flow streamlines and shear rate colour map.[18] (B) (a) Diagram of agarose–gelatin IPN hydrogel and the bonding of each layer *via* gelatin using carbodiimide crosslinking and confocal microscope images illustrating (b) the endothelialized microchannels occluded by sickle RBCs (stained in red; indicated by arrows), and (c) the resultant increased endothelial permeability and leakage of BSA-AF488 *in situ*.[19] (C) (a) Diagram illustrating assembly of photoablation-guided capillary growth in lithography-based microvessel devices. Confocal microscope images showing (b) stitched complete vessel network and (c) zoom-in constriction vessel in projected and cross-sectional views, (d) bright-field image of RBCs flowing through a constriction vessel (top) and spatial distribution of the blood cells accumulation after 20 min of perfusion with normal RBCs (middle) and infected RBCs (bottom) represented by heat map.[147]

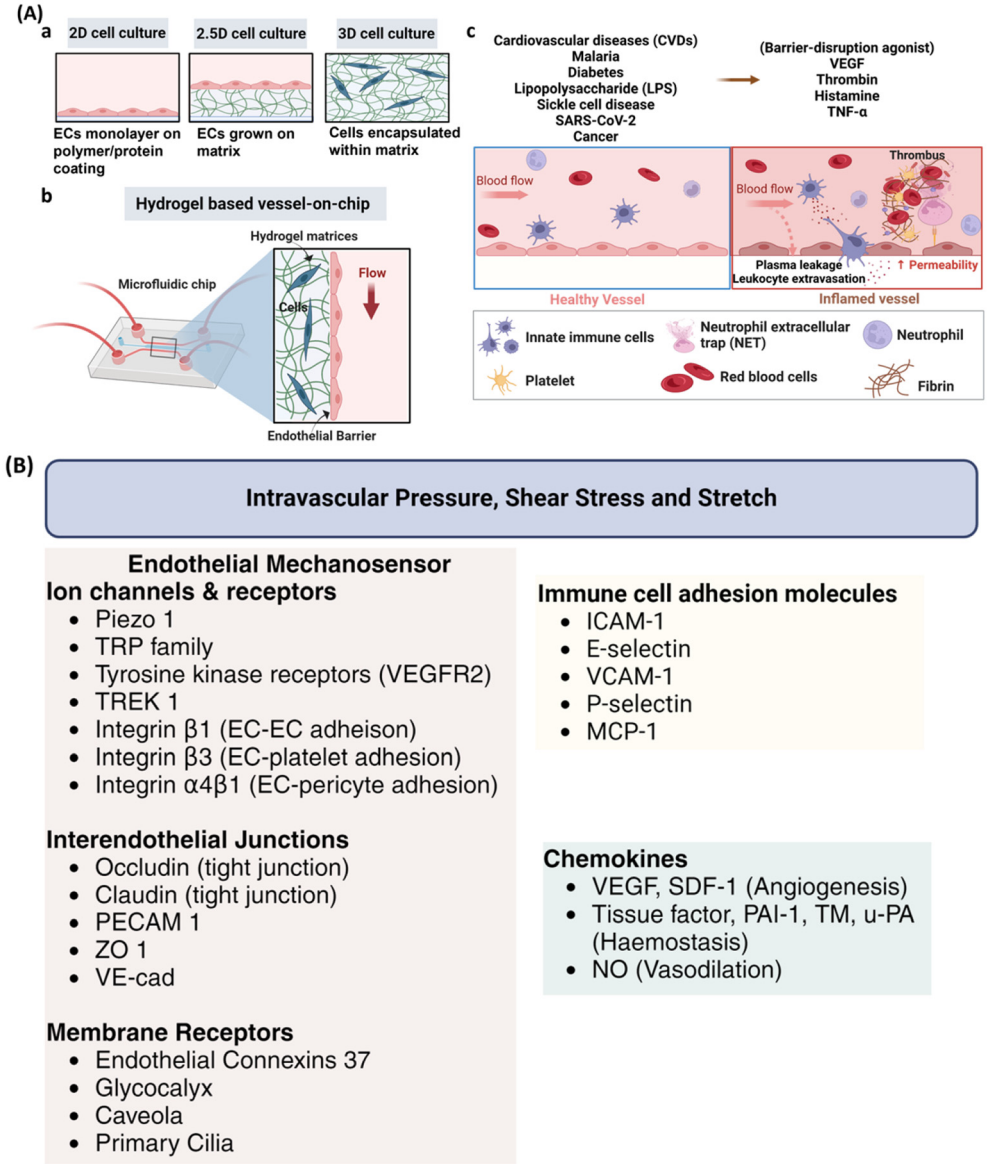

Fig. 10 (A) Schematic illustration of (a) cell culture grown on various substrates, (b) hydrogel-based microfluidic vessel-on-a-chip model, (c) vascular permeability and blood clotting in healthy vessel *vs.* injured vessel caused by trigger factors. (B) Diagram of endothelial cell's mechanotransduction pathway in response to haemodynamic signals. Created with BioRender.com. Abbreviations: TRP, transient receptor potential; TREK1, TWIK-related potassium channel-1; PECAM, platelet endothelial cell adhesion molecule; ZO-1, zonula occludens-1; ICAM, intercellular adhesion molecules; VCAM, vascular cell adhesion molecules; MCP-1, monocyte chemoattractant protein-1; VEGF, vascular endothelial growth factor; SDF-1, stromal cell-derived factor-1; PAI-1, plasminogen activator inhibitor-1; TM, thrombomodulin; TF, tissue factor; u-PA, urokinase type plasminogen activator; NO, nitric oxide.

4. Advancing thrombosis models: the role of bioprinting and perfusion technologies

4.1 The promise of 3D bioprinting in vascular modeling

The field of thrombosis research has been significantly advanced by the development of hydrogel-based microfluidic chips, which have successfully mimicked hollow circular lumens and adjustable flow patterns.[13,17,178] These models have provided valuable insights into the dynamics of blood flow and cellular interactions in thrombosis. However, they often fall short in replicating the full complexity of patient-specific vascular geometries and the concentric multilayer arrangements with varying elasticity found in native blood vessels. This limitation has paved the way for the emergence of 3D bioprinting as a promising solution in vascular modeling.

3D bioprinting, an innovative tissue engineering technology, offers the ability to precisely deposit living cells and biocompatible materials, creating intricate structures that closely

Table 2 Hydrogel materials used in fabrication of vascular hollow channel

Hydrogels	Fabrication techniques	Young's modulus	Resolution (channel size)	Ref.
Collagen	Soft lithography and injection moulding	NA	40–1000 μm	18
Collagen	Soft lithography and multiphoton ablation	NA	5–10 μm	147
Gelatin/GelMA Alginate/gelatin Alginate/GelMA	Casting and bonding *via* UV- or ionic-crosslinking	NA	160–1500 μm	15
F127DA and Irgacure	Casting and bonding *via* UV crosslinking	6.5 MPa	500 μm	137
Agarose/gelatin	Casting and bonding *via* carbodiimide crosslinking	5–50 kPa	20–80 μm	19
3% agarose	Casting and bonding *via* thermal crosslinking	19–32 kPa	50 μm × 70 μm (rectangular channel)	177
6% agarose and 0–200% sucrose crystals	Microneedle as template (0.38 mm ID, 0.6 mm OD)	14.7–129.8 kPa (varies upon sucrose concentration)	500 μm	138
Collagen	Acupuncture needle as template	NA	150–300 μm	17 and 178
Collagen	Tapered glass pipette or etched needle as template	260–1330 Pa	20–80 μm, 60–80 μm, 75–150 μm	133, 135, 139 and 179
Collagen/fibrin	Gelatin as sacrificial template	NA	6–50 μm	14
Silk and HRP/H_2O_2	Gelatin as sacrificial template	1–1000 kPa (varies upon silk's crystallinity)	100 μm	142
Gelatin/agarose/collagen	Alginate as sacrificial template	NA	20–500 μm	143
Gelatin/fibrinogen	18 G needle as template	1–10 kPa	650 μm	140
PEG-NB, RGD peptide, DTT or PEG-DT and LAP	UV-light photopatterning (transparent photomask film as template)	NA	~30 μm	146
PEGDA	Laser-based hydrogel degradation (virtual masks as template)	NA	3.28–8.86 μm	180

mimic natural vascular tissues.[181–185] This technology allows for the recreation of patient-specific geometries, incorporation of multiple cell types and biomaterials, and automated fabrication of diverse vascular models. The high-resolution spatial control, multi-material printing capabilities, and ability to create cell-laden constructs make 3D bioprinting particularly valuable for studying the complex, individualized nature of thrombotic events.

One of the key advantages of 3D bioprinting is its ability to achieve resolutions down to tens of micrometers, allowing for the creation of intricate vascular structures that closely resemble native blood vessels.[186,187] Moreover, the technology enables the use of different bioinks within a single print, facilitating the recreation of the heterogeneous nature of blood vessels.[74,181,188] This multi-material approach allows researchers to model the distinct layers of blood vessels, including the endothelium, smooth muscle layer, and adventitia, each with its specific cellular composition and mechanical properties.[74] Perhaps most importantly, 3D bioprinting allows for the direct incorporation of living cells into the printing process. This capability ensures that cells are precisely positioned within the construct, maintaining their viability and function.[185,189] The ability to create cell-laden vascular models opens up new possibilities for studying cell–cell and cell–matrix interactions in the context of thrombosis.

Furthermore, the customization potential of 3D bioprinting is particularly exciting for thrombosis research. Patient-specific data from medical imaging can be used to create personalized vascular models, potentially allowing for the study of thrombosis in the context of individual patient anatomies and pathologies. This level of personalization could be invaluable in developing tailored treatment strategies and understanding why some individuals are more prone to thrombotic events than others.[190]

4.2 Bioprinting techniques for vascular structures

Several bioprinting techniques have been developed to create anatomically accurate and perfusable 3D vessel models, each with its own set of advantages and challenges (Table 3). The main approaches include extrusion bioprinting, sacrificial bioprinting, and light-based bioprinting techniques.

4.2.1 Extrusion bioprinting. Extrusion bioprinting, including coaxial and triaxial approaches, allows for the creation of tubular constructs with tunable stiffness (Fig. 11A).[181,188,191–193] This method involves the continuous extrusion of bioink through a nozzle, with the potential for multiple concentric nozzles to create layered structures. The nozzle diameter, which typically ranges from 100 to 500 μm, significantly influences the resolution of the printed structures. Extrusion pressure can vary from 10 to 1000 kPa, depending on bioink viscosity, while print speeds usually fall between 1 and 50 mm s^{-1}, affecting both resolution and cell viability (Table 3).

One of the key advantages of extrusion bioprinting is its ability to create multi-layered vascular structures. For instance, Gao *et al.* demonstrated the creation of a triple-layered vascular construct using a triaxial nozzle, incorporating endothelial cells, smooth muscle cells, and fibroblasts in distinct layers.[194]

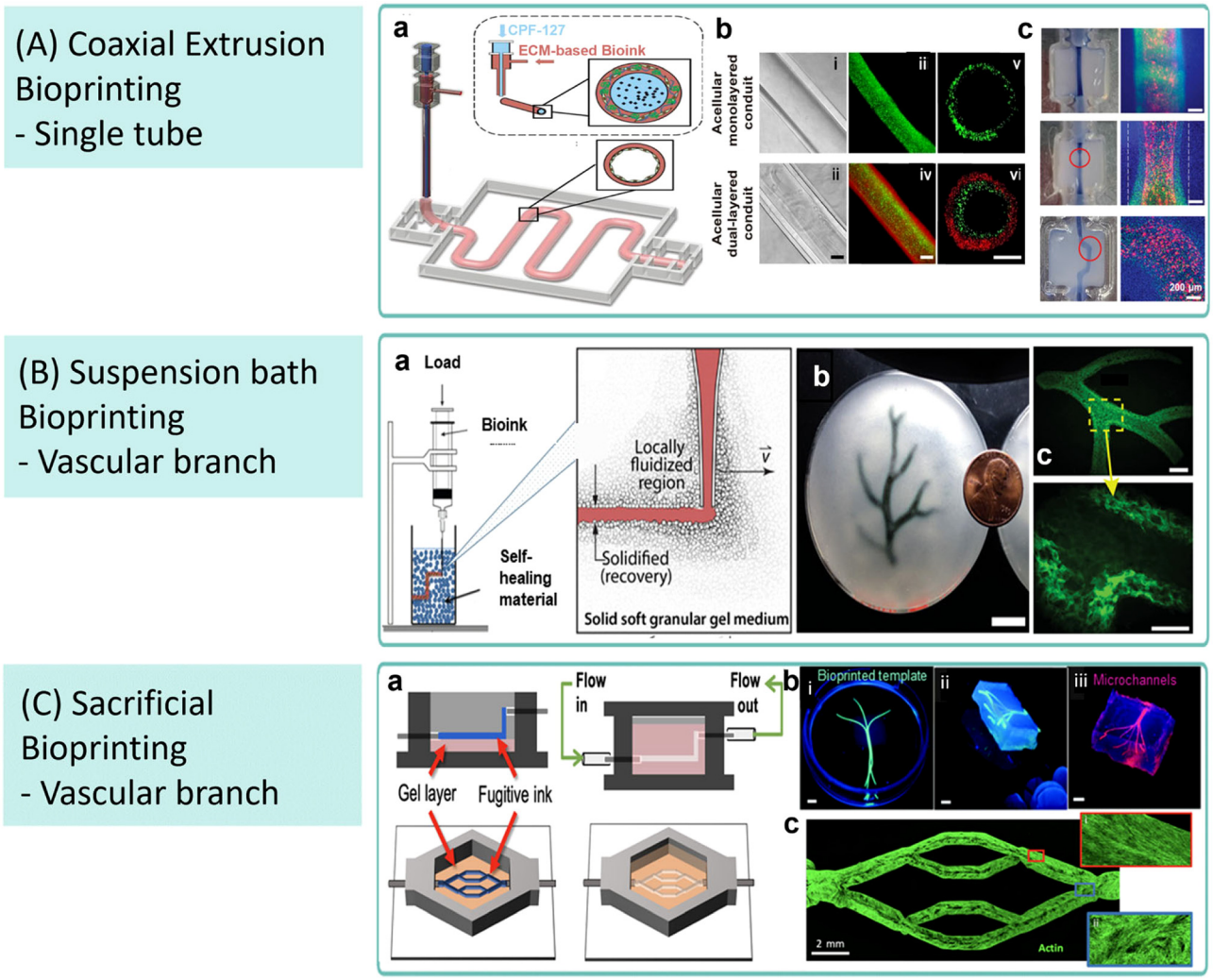

Fig. 11 Extrusion bioprinting using nozzles to produce hollow vascular structures. (A) (a) Schematic diagram of coaxial bioprinting giving rise to (b) hollow tubes with single/double wall,[181] (c) printed vessels with tunable geometries: straight (top), stenotic (middle), and tortuous (bottom) models (scale bar = 200 μm).[202] (B) (a) A schematic illustration of complex object that can be printed in a suspension bath where granular gel medium locally fluidizes while the nozzle moves and then rapidly solidifies around extruded structure, (b) photograph of a coronary arterial tree printed in alginate (black) which is embedded in gelatin slurry support bath (scale bar = 10 mm), (c) fluorescent microscopic images of the printed arterial tree with multiple bifurcations (top) (scale bar = 2.5 mm) and a zoomed-in view of the yellow inset box (bottom) showing well-defined vascular wall with hollow lumen (scale bar = 1 mm).[196,197] (C) (a) Schematics of microfluidic vascular network generated by sacrificial bioprinting using fugitive ink, (b) photographs of (i) bioprinted agarose gel fibers template (green), (ii) the template embedded in a GelMA hydrogel and (iii) the perfusable branched network (red) after removal of the template (scale bar = 3 mm),[203] (c) fluorescent microscopic images of cytoskeletal morphology of ECs (scale bar = 2 mm) with zoom-in views of highly aligned actin fibers in straight regions of the vascular bed (red inset) and misaligned actin in bifurcated regions (blue inset).[204]

This approach closely mimics the natural structure of blood vessels, potentially leading to more physiologically relevant models for thrombosis research.

However, extrusion bioprinting is not without its challenges. The process can subject cells to potentially damaging shear stress during extrusion, with stress levels in the nozzle ranging from 0.1 to 100 kPa.[198] This stress can affect cell viability, with reported rates ranging from 40% to 95%, depending on cell type and printing conditions.[199–201] Additionally, the method is limited in resolution, typically producing lumen diameters greater than 300 μm,[188] which may not be suitable for modeling smaller blood vessels or capillaries and use of nozzle limits vessel geometry to a single tube.

4.2.2 Suspension bath bioprinting. To provide branched vascular network, the extrusion 3D printing can be embedded within support bath in which hydrogel slurries serving as mechanical support for shape fidelity of printed channels, preventing collapse (Fig. 11B). Materials with both shear-thinning and self-healing characteristics that can recover after removal of an applied shear stress (*i.e.*, movement of a nozzle in extrusion bioprinting) have been developed to be used as support bath to physically confine mechanically week bioink after

extrusion (Table 3).[195–197] As such, optimisation of materials that can be used as a support bath to suit a range of extruded bioink as well as to improve print fidelity and resolution is an area of research interest to fabricate complex, well-defined vascular structures. Bhattacharjee *et al*. demonstrated the capability of their granular suspension medium to fabricate an interconnected 3D microvascular network with narrow channels down to 100 μm in diameter.[195]

4.2.3 Sacrificial bioprinting. Sacrificial bioprinting has emerged as a technique to create more complex, branched networks (Fig. 11C). This method involves printing a sacrificial material, such as agarose,[203] gelatin,[205,206] sintered carbohydrate[186] or pluronic F-127,[182,207] that is later removed to create hollow channels. The process typically involves printing the sacrificial material in the desired vascular pattern, casting a cell-laden hydrogel around the sacrificial structure, and then removing the sacrificial material through dissolution, melting, or aspiration (Table 3).

Kolesky *et al.* demonstrated the power of this technique by creating a perfusable vascular network with channel diameters as small as 150 μm.[21,208] They used Pluronic F127 as the sacrificial ink, which was printed and then evacuated at 4 °C, leaving behind open channels that were subsequently endothelialized. This approach allows for the creation of more complex vascular geometries than is typically possible with direct extrusion methods.

While sacrificial bioprinting offers finer control over channel geometry and the ability to create intricate vascular networks, it comes with its own set of challenges. The multistep process can be time-consuming and requires careful optimization to ensure complete removal of the sacrificial material without damaging the surrounding cell-laden hydrogel. Additionally, there is always the risk of residual sacrificial material affecting the biological properties of the final construct.

4.2.4 Light-based bioprinting. Light-based bioprinting techniques, such as digital light processing (DLP) and volumetric bioprinting (VBP), have gained attention for their ability to produce high-resolution, complex vascular networks.[184,185,189] These methods offer superior design freedom and the ability to create out-of-plane branches rapidly, making them particularly suited for modeling complex vascular geometries (Fig. 12).

Digital light processing (DLP) uses a digital micromirror device to selectively crosslink photosensitive bioinks. This technique can achieve resolutions of 10–100 μm in the x–y plane and 25–100 μm in the z-direction, allowing for the creation of highly detailed vascular structures. DLP also offers rapid production speeds, with print speeds up to 100 mm h^{-1}. Levato *et al.* demonstrated the potential of this technique by creating a perfusable arterial tree model with channel diameters down to nearly 60 μm, maintaining high fidelity to the original design.[183]

Volumetric bioprinting (VBP) takes a different approach, forming entire 3D structures simultaneously by projecting light patterns into a volume of photosensitive bioink. This technique can produce complex structures in seconds to minutes, regardless of object height, with resolutions ranging from 80–400 μm depending on the setup and materials used.[184,185,213] Falandt *et al.* showcased the speed and versatility of VBP by creating complex vascular structures in less than 30 seconds, with negative feature sizes down to approximately 175 μm (Table 3).[214]

Despite their advantages, light-based bioprinting techniques face challenges such as potential channel clogging due to light scattering[212] and, in some cases, lower mechanical stability.[184,213] The penetration depth of light and the presence of photoabsorbers in the bioink must be carefully balanced to achieve the desired resolution and structural integrity.[215] Additionally, the choice of photoinitiators and the light exposure time must be optimized to ensure cell viability in cell-laden constructs.[216] Benefiting from nozzle-free mechanism and there is no external mechanical forces (*i.e.*, shear stress) imposed on the living cells during printing, the cytotoxicity of encapsulated cells usually come from the radicals generated during crosslinking and thermal/radiative stress from the light source. Nevertheless, it still demonstrates high cell viability exceeding 90%.[199,217]

4.2.5 Hybrid approaches. Recognizing the limitations of individual techniques, researchers have begun to explore hybrid approaches that combine different bioprinting technologies to leverage their respective strengths and overcome individual limitations. Ching *et al.* developed a novel biofabrication methodology combining 3D printing of rigid frames, bioprinting of porous molds by DLP, and ionic-UV crosslinking of bioinks by coaxial microfluidic setup (Fig. 13A).[74] This approach generates free-standing, multilayered vascular branches in different geometries capable of recapitulating patient-specific cardiovascular diseases. The resulting constructs exhibited tunable mechanical properties, with Young's moduli ranging from 10 kPa to 1.7 MPa, matching the elasticity of various native blood vessels.

Similarly, Größbacher *et al.* combined melt electrowriting (MEW) with VBP to offer multi-material and multilayered vascular structures with mechanically reinforced printed constructs (Fig. 13B).[184] The MEW process created a fibrous scaffold with precise fiber placement (5–50 μm diameter fibers), which was then embedded within a cell-laden hydrogel through VBP. This hybrid approach resulted in vascular constructs with enhanced mechanical properties, with Young's moduli ranging from 3.2 to 10.8 kPa, depending on the MEW mesh pattern. These hybrid methods represent a promising direction for creating more physiologically relevant vascular models, offering improved mechanical properties, higher resolution, and the ability to incorporate multiple cell types in distinct spatial arrangements.

4.3 Bioinks for vascular modeling

The choice of bioink is crucial in creating advanced vascular models. Researchers must balance mechanical properties, biocompatibility, and printability when selecting materials. A wide range of bioinks have been explored, from natural poly-

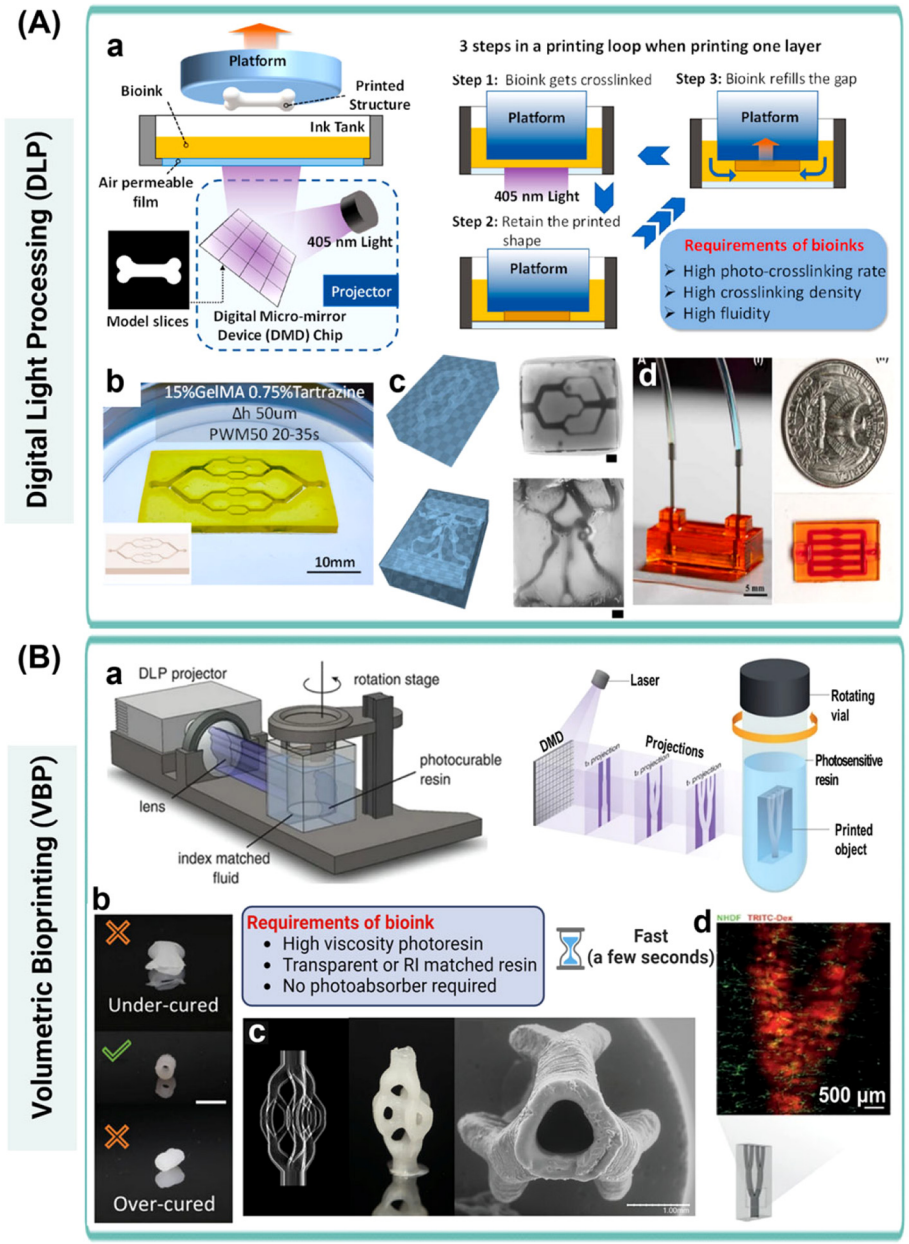

Fig. 12 Fabrication of hollow tubular bioprinted structures to model complexity of vascular network by light-based bioprinting techniques. (A) (a) Schematic pictures showing steps involved in layer-by-layer based DLP bioprinting, (b) DLP printed vasculature structure,[209] (c) STL models (blue) and stereomicroscopic images of branched microfluidic network and human Willis circuit based on angiographic 3D data. Scale bars = 1 mm.[183] (d) pictures of DLP printed ready-to-use microfluidic chip.[210] (B) (a) Schematic representation of VBP demonstrating that an entire 3D object is simultaneously solidified by irradiating a volume of photoresins in a glass vial from multiple angles with dynamic light patterns.[189,211] (b) Pictures of volumetrically printed vascular construct under different projection time: under-cured (*i.e.*, collapsed channel (top)), over-cured (*i.e.*, clogged channel) and optimal-cured (*i.e.*, mechanically stable and patent channel (middle)). Scale bar = 5 mm. (c) Projection model, photo, and SEM image of triple vasculature structure with a central channel of 900 μm and a wall thickness of 400 μm. Scale bar 1 mm,[212] (d) confocal image of bifurcated model encapsulated with human dermal fibroblast (green) and perfused with TRITC-dextran (red) in channel (scale bar = 500 μm).[189]

mers like gelatin and alginate to synthetic materials like polyethylene glycol derivatives. The viscosity of these bioinks typically ranges from 30 to 6×10^7 mPa s^{-1},[219] depending on the printing method. Shear-thinning behavior is important for extrusion-based methods to reduce cell damage and to maintain shape fidelity, while crosslinking mechanisms can be physical (*e.g.*, temperature-sensitive) or chemical (*e.g.*, photocrosslinking).

Semi-synthetic polymers like gelatin methacryloyl (GelMA) are popular due to their biocompatibility and cell-adhesive properties. GelMA-based bioinks have been used to create vascular constructs with Young's moduli ranging from 0.5 to 110

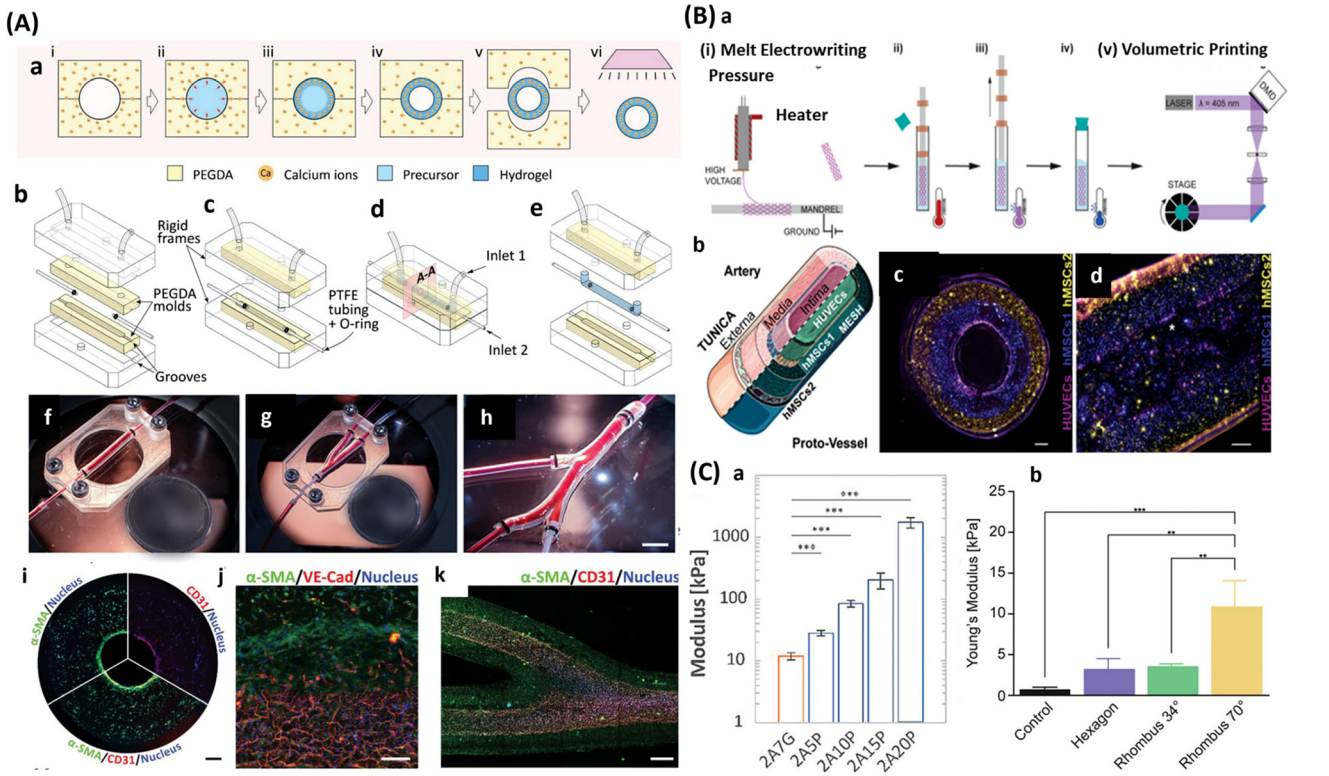

Fig. 13 Hybrid bioprinting technologies. (A) Microfluidic enabled molding technique. (a–e) Diagrammatic illustration of steps involved in the molding and coaxial biopriting, that generates (i–iii) vasculatures in different geometries and (f–k) confocal images of the multilayered vascular construct with endothelialised channels surrounded by smooth muscle cells (scale: (iv) 200 μm, (v) 100 μm, (vi) 500 μm).[74] (B) (a) Graphical representation of melt electrowriting (MEW) and volumetric printing (VBP). (i) Fabrication of tubular melt electrowritten scaffolds on a rod and (ii)–(iv) their subsequent incorporation into the volumetric printing process by placing the MEW mesh into a vial of GelMA; (v) volumetric printing. (b) Picture of native artery in comparison with VolMEW printed proto-vessel. (c) Perpendicular and (d) longitudinal cross-sectional fluorescence images of a three-layer VolMEW printed tubular construct with hMSCs (blue and yellow) in the gel layer and a HUVEC-seeded lumen (magenta).[184] (C) Young's modulus of printed vessel (a) by microfluidic molding technique using a mixture of bioink such as alginate (A), GelMA (G) and PEGDA (P) and (b) by MEW with different patterns of meshes and GelMA-only control.[184]

kPa, depending on concentration and crosslinking parameters.[216] Synthetic polymers like poly(ethylene glycol) diacrylate (PEGDA) offer greater control over mechanical properties. PEGDA-based bioinks have been used to create vascular models with Young's moduli ranging from 24 kPa to 1.18 MPa.[210]

Composite bioinks, combining natural and synthetic polymers, are increasingly used to leverage the advantages of both. For example, a GelMA/PEGDA composite bioink developed by Ching *et al.* achieved a Young's modulus of 1.7 MPa, closely matching that of native blood vessels (Fig. 13C).[220] The mechanical properties of these bioinks can vary widely, from soft gels with Young's moduli in the kPa range to stiffer materials reaching several MPa, allowing for the mimicry of different vascular tissues (Table 4). This versatility enables the creation of models that can accurately represent various parts of the vascular system, from large arteries to small capillaries.

4.4 Challenges in perfusion of bioprinted vascular models

While bioprinting has significantly advanced the creation of complex vascular structures, integrating these models with perfusion systems presents a new set of challenges. The mechanical fragility of hydrogel-based constructs often makes them too soft to withstand physiological pressures, which typically range from 60–120 mmHg in arteries.[17,224] Interface leakage is a common issue when connecting soft hydrogel structures to rigid tubing, and ensuring consistent flow throughout complex, branched structures is challenging, particularly in models with varying channel diameters. Maintaining the integrity of bioprinted structures during extended perfusion periods (days to weeks) remains a significant hurdle.

The operation of a continuous perfusion system in hydrogel-based chips is much more complicated than that of PDMS devices, where static friction between tubing and PDMS offers a robust, tight-seal connection for pressurized liquid flow.[224] In PDMS devices, leak-free connections can typically withstand pressures up to 200 kPa, whereas hydrogel-based systems often fail at much lower pressures. Connecting hydrogels to external pumps can be cumbersome due to severe mechanical strains in the hydrogel, leading to breakage and fluid leakage in long-term flow

Table 3 Various bioprinting technologies to fabricate vascular conduits

Bioprinting techniques	Advantages	Disadvantages	Resolution (channel size)
Extrusion bioprinting	Able to print multi-layered vascular construct[181]	Limited resolution, low printing speed, low cell viability,[199] limited vascular geometries	~300 μm (ref. 193)
Sacrificial bioprinting	Able to print branched vascular structures by removal of fugitive ink[203,207]	Multi-step procedures and time-consuming	~150 μm (ref. 21)
Embedded bioprinting	Able to print branched vascular structures by mechanical support for shape fidelity[195,197,218]	Requires self-healing hydrogel bath with special material characteristics[195,197]	~100 μm (ref. 195)
DLP	Able to print pre-programmed patient-specific complex vascular structures,[183,190] high resolution[183]	Channel clogging from light scattering,[215] thermal/radiative stress to cells from light source[199,217]	~60 μm (ref. 183)
VBP	Able to print complex vascular network, fast printing speed[214]	Channel clogging from light scattering,[212] limited bioink/resin,[213] low mechanical strength[184]	~200 μm (ref. 214)

Table 4 Various bioink used in bioprinting of vascular structure

Bioink for vascular model	Biofabrication techniques	Young's modulus	Resolution (channel size)	Ref.
5% GelMA and 0.2% PI	Sacrificial bioprinting (Pluronic as template)	0.65–0.8 kPa (varies upon UV irradiation time)	3 mm	182
PEGDA and Irgacure 2959, agarose, silk, fibrin	SLS-CaST (laser-sintered carbohydrate as template)	~100 kPA (PEGDA), 200–400 kPa (agarose), 3–10 kPa (silk), 1–10 kPa (fibrin)	~300 μm	186
LTS-GelMA, LTS-GelNB and Ru/SPS, PA	DLP	0.99–6.81 kPa (LTS-GelMA) 1.38–55.63 kPa (LTS-GelNB)	64 ± 7 μm (LTS-GelMA) 95 ± 21 μm (LTS-GelNB)	183
10–15% GelMA, tartrazine and LAP	DLP	0.04–0.4 MPa	NA	209
GelMA/PEGDA/LAP and orange food dye	DLP	24 kPa–1180 kPa	~250 μm	210
5% GelMA, LAP and IDX	DLP	0.5 kPa–2 kPa (varies upon encapsulated cell densities)	250–600 μm	216
Alginate/gelatin	Coaxial bioprinting	142.8–538 kPa	800 μm–5 mm	181
Alginate/polylysine (heparin and YIGSR coating)	Coaxial bioprinting	1–5 MPa (varies upon ratio of alginate to polylysine)	630–1300 μm	221
GelMA/alginate/MC/ PEG-Tyr and Rb/SPS	Coaxial bioprinting	8–15 kPa	~320 μm	193
Alginate	Coaxial bioprinting (nozzle: 700 μm inner diameter)	N/A	500 μm–2 mm (varies upon extrusion flow rates and printhead speeds)	188
Sacrificial gelatin as core- and collagen as shell-material	Embedded bioprinting (gelatin–chitosan microparticles in prepolymer collagen solution as support bath)	NA	0.29–1.57 mm (varies upon printing speed)	218
Alginate/GelMA Alginate/PEGDA	Molding and microfluidics co-axial printing	10 kPa–1.7 MPa	2–10 mm	220
PTHF-DA	Multiphoton polymerization	6 MPa–30 MPa	18 μm	222
GelMA/SPELA/PEGDMA and PEGDA	Sacrificial bioprinting (agarose as template)	~150 kPa	250–1000 μm	203
5% GelMA and LAP	VBP	5–8 kPa (varies upon LAP amount)	0.9–1.2 mm	185
PCL	VBP	66–233 MPa	900 μm	212
GelNB/PEG4SH and LAP	VBP	40 Pa–15 kPa (varies upon polymer content, thiol–ene ratio, and thiolated crosslinker)	200 μm	189
GelNB/DDT and LAP	VBP	2.52–6.30 kPa (varies upon thiol to norbornene ratio)	176 ± 36.34 μm	214
nPVA/PEG2SH/gelatin/ pyrogallol and LAP	VBP	2.7–25 kPa (varies upon polymer concentration)	0.85–1.23 mm	223
8% GelMA and 0.01% LAP	MEW and VBP	3.2–10.8 kPa (varies upon pattern of MEW mesh)	15 mm	184
20% PEGDA, LAP and PA	Custom-designed projection stereolithography	NA	0.4–1 mm	187

Abbreviations: PI, photoinitiator; PA, photoabsorber; SLS-CaST, selectively laser-sintered carbohydrate sacrificial templating; LTS-GelMA, low temperature soluble gelatin methacryloyl; LTS-GelNB, low temperature soluble gelatin norbornene; IDX, iodixanol; DTT, 2,2′-(ethylenedioxy) diethanethiol; PEGDA, polyethylene glycol diacrylate; PTHF-DA, polytetrahydrofuranether-diacrylate; SPELA, star poly(ethylene glycol-*co*-lactide) acrylate; PEGDMA, poly(ethylene glycol)dimethacrylate; PEG4SH, 4-arm-PEG-thiol; LAP, lithium phenyl(2,4,6-trimethylbenzoyl)phosphinate; PCL, polycaprolactone; Ru/SPS, ruthenium/sodium persulfate; nPVA, norbonene-functionalised polyvinyl alcohol; NA, not assessed.

studies.[17,224] The mismatch in mechanical properties between soft hydrogels (Young's modulus typically <100 kPa) and rigid tubing (Young's modulus >1 GPa) creates stress concentrations at the interface, leading to failure under prolonged perfusion.

4.5 Innovative solutions for perfusable bioprinted vessels

To address these perfusion challenges, researchers have developed several innovative solutions. Kinstlinger *et al.* created an open-source design for a customizable perfusion bioreactor chamber compatible with a wide range of engineered tissues (Fig. 14A).[16] This system allows for controlled perfusion of complex vascular networks, long-term culture of bioprinted constructs (up to several weeks), and integration with imaging systems for real-time monitoring. The chamber design incorporates adjustable compression to secure the hydrogel construct, multiple inlet/outlet ports for complex perfusion patterns, and a transparent window for real-time imaging. This system has demonstrated the ability to maintain stable perfusion of bioprinted vascular networks for over 14 days, with flow rates up to 1 mL min^{-1} and pressures up to 150 mmHg.

Abbasi *et al.* developed a 3D printed "pop-it" connector that utilizes the elasticity of hydrogels rather than static friction.[224] This design enables stable, long-term liquid flow (tested for up to 7 days), pressure control comparable to PDMS-based devices (up to 200 kPa), and reduced risk of leakage at the hydrogel-tubing interface. The connector features a tapered interface that matches the elasticity of the hydrogel, an O-ring seal for additional leak prevention, and customizable dimensions to fit various hydrogel constructs. This innovative connector design has shown a 90% success rate in maintaining leak-free connections over a 7-day perfusion period, significantly outperforming traditional connection methods.

Integration of bioprinted constructs with microfluidic devices offers precise control over flow patterns and shear stress (0.1–10 dyn cm^{-2}), miniaturization for high-throughput experiments (up to 96 parallel channels),[226] and the ability to simulate both physiological and pathological flow conditions.[87,227] Perfusion bioreactors coupled with microfluidic devices can be useful for miniaturizing vascularized tissue systems for higher throughput cardiovascular experiments (Fig. 14B). These systems typically incorporate programmable syringe pumps for precise flow control, inline pressure sensors

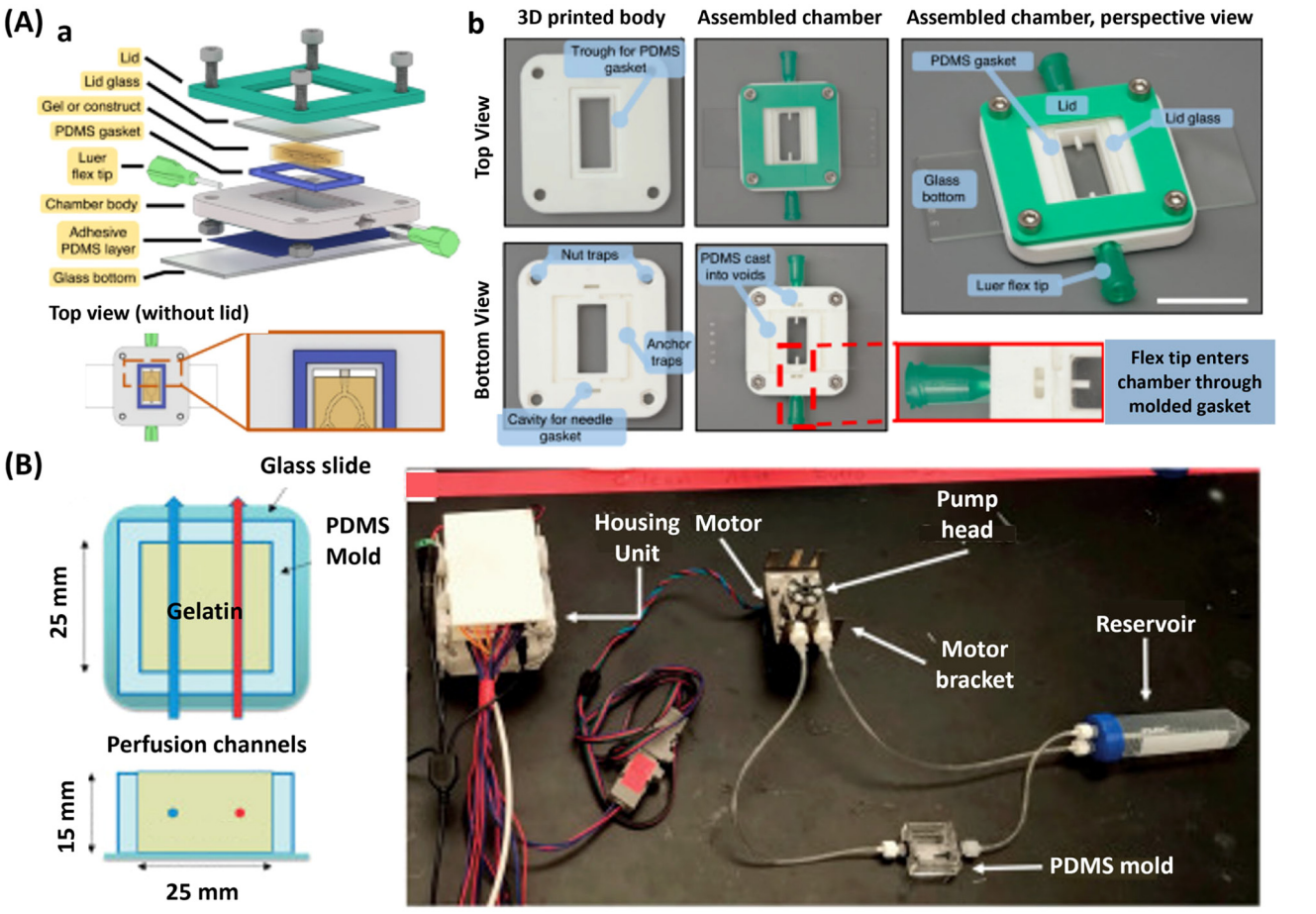

Fig. 14 (A) (a) Diagram and (b) photos illustrating components involved in a custom-made bioreactor design for perfusable vascular culture system. (B) Graphical representation of hydrogel construct with perfusion channels in a PDMS mold and custom perfusion system setup.[16,225]

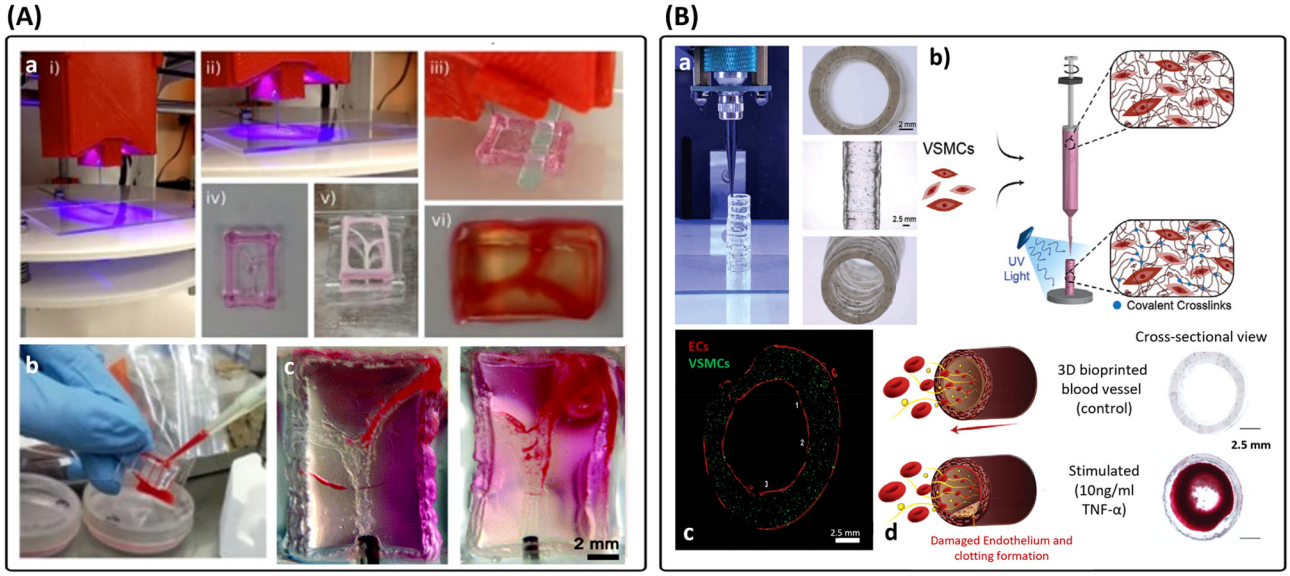

Fig. 15 3D thrombosis model fabricated by bioprinting. (A) (a) Photographs showing (i–vi) experimental steps of sacrificial bioprinting using Pluronic as template for channel and GelMA in bulk hydrogel, (b) perfusion of human whole blood by pipetting it into the endothelialized microchannels and (c) the bioprinted thrombosis-on-chip model.[182] (B) (a) Photographs and (b) diagram of extrusion bioprinting to fabricate 3D bioprinted vascular model, (c) endothelialised 3D vascular model with ECs and VSMC co-culture, staining with different cell tracker (scale bar = 2.5 mm), (d) schematics illustrating clotting formation upon endothelial injury stimulated by TNF-α.[22]

for real-time monitoring, and temperature and gas exchange controls for physiological conditions. Wang *et al.* demonstrated a microfluidicbioprinted vascular conduit system that are capable of maintaining physiological shear stress (1-2Pa) and stable for up to 3 days without leakage, enabling future studies of endothelial function and thrombosis.[181]

4.6 Applications in thrombosis research

The advanced bioprinted vascular models, when combined with perfusion systems, offer unique opportunities for thrombosis research. These models can give rise to diseased models that represent thrombo-inflammatory responses upon inflammatory mediator stimulation and blood perfusion.[22,182,184] This capability provides a significant advantage over animal models for studying vascular diseases, thrombotic mechanisms, and drug screening.

Zhang *et al.* demonstrated the creation of a 3D bioprinted thrombosis model using sacrificial bioprinting (Fig. 15A).[182] This model allowed for perfusion of human whole blood through endothelialized microchannels, real-time visualization of thrombus formation, and quantification of platelet adhesion and fibrin deposition. The model successfully recapitulated key features of thrombosis, including shear-dependent platelet adhesion (0.1–40 dyn cm^{-2}), von Willebrand factor-mediated platelet tethering, and fibrin network formation.

Similarly, Gold *et al.* developed a 3D bioprinted vascular model with co-cultured endothelial cells and vascular smooth muscle cells, allowing for the investigation of clotting formation upon endothelial injury stimulated by TNF-α (Fig. 15B).[22] This model demonstrated increased endothelial permeability following TNF-α stimulation, enhanced platelet adhesion and aggregation at injury sites, and differential responses to anti-thrombotic drugs.

These bioprinted thrombosis models offer several advantages over traditional *in vitro* systems, including a more physiologically relevant 3D architecture, the ability to incorporate multiple cell types in defined spatial arrangements, control over vascular geometry and local hemodynamics, and the potential for high-throughput drug screening.

5. Conclusion and future outlook

The field of thrombosis research has undergone significant advancements in recent years, driven by the need for more physiologically relevant models that can accurately recapitulate the complex interplay of factors involved in Virchow's triad. The transition from traditional 2D cell cultures and animal models to sophisticated *in vitro* systems has opened new avenues for understanding thrombosis mechanisms and developing targeted therapies.

The evolution of microfluidic technologies, from PDMS-based devices to hydrogel-based systems, has greatly enhanced our ability to mimic the native vascular microenvironment. These platforms offer precise control over hemodynamic conditions, enabling researchers to study the effects of shear stress and flow patterns on endothelial function and thrombus formation. The incorporation of hydrogels as biomimetic matrices has further improved the physiological relevance of these models by providing a 3D microenvironment that better represents the extracellular matrix of blood vessels.

The emergence of 3D bioprinting technologies represents a significant leap forward in creating complex, multi-layered vascular structures. This approach allows for the fabrication of patient-specific vascular geometries and the incorporation of multiple cell types, paving the way for personalized thrombosis models. The integration of these bioprinted constructs with microfluidic systems has resulted in advanced "vessel-on-a-chip" platforms that offer unprecedented opportunities for studying thrombosis under controlled, physiologically relevant conditions.

Looking to the future, the integration of advanced bioprinting techniques with sophisticated perfusion systems holds great promise for thrombosis research. Efforts should focus on several key areas:

1. Improving the mechanical properties of bioprinted vessels to better withstand physiological pressures. This may involve developing new composite bioinks or incorporating reinforcing structures to create vessels that can maintain their integrity under physiological flow conditions.

2. Developing standardized perfusion systems for bioprinted constructs. This could include modular designs that can accommodate a variety of vascular geometries and flow conditions, making it easier for researchers to adopt and utilize these advanced models.

3. Creating multi-organ models that incorporate perfusable vascular networks. This would allow for the study of systemic effects on thrombosis and the interaction between different organ systems, providing a more comprehensive understanding of thrombotic disorders.

4. Enhancing the long-term stability of bioprinted vascular models under continuous perfusion. This may require innovations in hydrogel chemistry and perfusion system design to maintain construct integrity over weeks to months, enabling studies of chronic conditions and long-term drug effects.

5. Incorporating patient-specific cells and geometries for personalized medicine applications. This could involve using induced pluripotent stem cells (iPSCs) derived from patients and 3D imaging data to create truly personalized thrombosis models, paving the way for individualized risk assessment and treatment strategies.

6. Integrating advanced sensing technologies for real-time monitoring of thrombotic events. This might include incorporating biosensors or microelectrodes into the bioprinted constructs, allowing for continuous, non-invasive monitoring of thrombosis progression and resolution.

7. Developing high-throughput platforms for drug screening and toxicity testing. This could involve creating arrays of miniaturized vascular models for parallel testing of multiple compounds, accelerating the drug discovery and development process for antithrombotic therapies.

As these technologies continue to evolve, they will enable the creation of increasingly physiologically relevant models for studying thrombosis, screening potential therapies, and developing personalized medicine approaches. The ability to recreate patient-specific vascular geometries and flow conditions will provide unprecedented insights into the complex, individualized nature of thrombotic events, potentially leading to more effective prevention and treatment strategies.

Data availability

No primary research results, software or code have been included and no new data were generated or analysed as part of this review. All information discussed in this review is based on previously published literature, which is cited throughout the text.

Conflicts of interest

There are no conflicts to declare.

Acknowledgements

This work was supported by the NSW Cardiovascular Capacity Building Program (Early-Mid Career Researcher Grant – L. A. J.; H22/98586 – K. L.); MRFF Cardiovascular Health Mission Grants (MRF2016165 – L. A. J.; MRF2023977 – L. A. J.) and MRFF Early to Mid-Career Researchers Grant (MRF2028865 – L. A. J.); National Heart Foundation Vanguard Grant (106979 – L. A. J.); University of Sydney Proof-of-Concept Fund (STEM stream G225913 – L. A. J.). Lining Arnold Ju is a Snow Medical Research Foundation Fellow (2022SF176) and a National Heart Foundation Future Leader Fellow Level 2 (105863); Khoon Lim is an Australian Research Council Future Fellow (FT230100249).

The authors would like to thank Zihao Wang, Sihao Wang, Zhao (Jeff) Wang and Yanyan Liu for the advice on structuring of this paper and illustration.

References

1 G. Alkarithi, C. Duval, Y. Shi, F. L. Macrae and R. A. S. Ariëns, *Arterioscler., Thromb., Vasc. Biol.*, 2021, **41**, 2370–2383.
2 T. Watson, E. Shantsila and G. Y. H. Lip, *Lancet*, 2009, **373**, 155–166.
3 M. Wadman, *Science*, 2023, **379**, 127–128.
4 U.S. Centers, for Disease Control and Prevention (CDC), Heart Disease Facts, **https://www.cdc.gov/heart-disease/data-research/facts-stats/index.html**, (accessed 1 December 2024).
5 World Heart Federation, Deaths from cardiovascular disease surged 60% globally over the last 30 years: report, **https://world-heart-federation.org/news/deaths-from-cardiovascular-disease-surged-60-globally-over-the-last-30-years-report/**, (accessed 1 December 2024).
6 World Health Organization, Cardiovascular diseases (CVDs), **https://www.who.int/news-room/fact-sheets/detail/**

cardiovascular-diseases-(cvds), (accessed 1 December 2024).
7 D. Wang, T. Brady, L. Santhanam and S. Gerecht, *Nat. Cardiovasc. Res.*, 2023, **2**, 718–732.
8 T. V. Colace, G. W. Tormoen, O. J. T. McCarty and S. L. Diamond, *Annu. Rev. Biomed. Eng.*, 2013, **15**, 283–303.
9 C. E. Hansen and W. A. Lam, *Anal. Chem.*, 2017, **89**, 11881–11892.
10 Y. Zhang, S. Z. Ramasundara, R. E. Preketes-Tardiani, V. Cheng, H. Lu and L. A. Ju, *Front. Cardiovasc. Med.*, 2021, **8**, 766513.
11 R. Jianfang, W. Zhao, D. Nixon, C. Wenlong and A. J. Lining, *Microstructures*, 2024, **4**, 2024037.
12 E. Westein, A. D. van der Meer, M. J. E. Kuijpers, J.-P. Frimat, A. van den Berg and J. W. M. Heemskerk, *Proc. Natl. Acad. Sci. U. S. A.*, 2013, **110**, 1357–1362.
13 J. C. Kohn, D. W. Zhou, F. Bordeleau, A. L. Zhou, B. N. Mason, M. J. Mitchell, M. R. King and C. A. Reinhart-King, *Biophys. J.*, 2015, **108**, 471–478.
14 A. P. Golden and J. Tien, *Lab Chip*, 2007, **7**, 720–725.
15 J. Nie, Q. Gao, Y. Wang, J. Zeng, H. Zhao, Y. Sun, J. Shen, H. Ramezani, Z. Fu, Z. Liu, M. Xiang, J. Fu, P. Zhao, W. Chen and Y. He, *Small*, 2018, **14**, 1802368.
16 I. S. Kinstlinger, G. A. Calderon, M. K. Royse, A. K. Means, B. Grigoryan and J. S. Miller, *Nat. Protoc.*, 2021, **16**, 3089–3113.
17 W. J. Polacheck, M. L. Kutys, J. B. Tefft and C. S. Chen, *Nat. Protoc.*, 2019, **14**, 1425–1454.
18 Y. Zheng, J. Chen and J. A. López, *Nat. Commun.*, 2015, **6**, 7858.
19 Y. Qiu, B. Ahn, Y. Sakurai, C. E. Hansen, R. Tran, P. N. Mimche, R. G. Mannino, J. C. Ciciliano, T. J. Lamb, C. H. Joiner, S. F. Ofori-Acquah and W. A. Lam, *Nat. Biomed. Eng.*, 2018, **2**, 453–463.
20 Y. Liu, T. Huang, N. A. Yap, K. Lim and L. A. Ju, *Bioact. Mater.*, 2024, **42**, 328–344.
21 D. B. Kolesky, R. L. Truby, A. S. Gladman, T. A. Busbee, K. A. Homan and J. A. Lewis, *Adv. Mater.*, 2014, **26**, 3124–3130.
22 K. A. Gold, B. Saha, N. K. Rajeeva Pandian, B. K. Walther, J. A. Palma, J. Jo, J. P. Cooke, A. Jain and A. K. Gaharwar, *Adv. Healthcare Mater.*, 2021, **10**, e2101141.
23 S. Chatterjee, *Front. Physiol.*, 2018, **9**, 524.
24 S. Zhang, G. Xu, J. Wu, X. Liu, Y. Fan, J. Chen, G. Wallace and Q. Gu, *Small Methods*, 2024, **8**, 2300685.
25 C. J. Mandrycky, C. C. Howard, S. G. Rayner, Y. J. Shin and Y. Zheng, *J. Mol. Cell. Cardiol.*, 2021, **159**, 1–13.
26 K. M. Gray and K. M. Stroka, *Semin. Cell Dev. Biol.*, 2017, **71**, 106–117.
27 N. G. dela Paz and P. A. D'Amore, *Cell Tissue Res.*, 2009, **335**, 5–16.
28 W. C. Aird, *Circ. Res.*, 2007, **100**, 158–173.
29 A. M. Malek, S. L. Alper and S. Izumo, *J. Am. Med. Assoc.*, 1999, **282**, 2035–2042.
30 W. C. Aird, *J. Thromb. Haemostasis*, 2005, **3**, 1392–1406.
31 X. Su, L. Huang, Y. Qu, D. Xiao and D. Mu, *Front. Cell. Neurosci.*, 2019, **13**, 519.
32 Y. Fu, Y. Zhou, K. Wang, Z. Li and W. Kong, *Circ. Res.*, 2024, **134**, 931–949.
33 C. Tomasina, T. Bodet, C. Mota, L. Moroni and S. Camarero-Espinosa, *Materials*, 2019, **12**, 2701.
34 A. Lesman, D. Rosenfeld, S. Landau and S. Levenberg, *Adv. Drug Delivery Rev.*, 2016, **96**, 176–182.
35 A. Hooglugt, O. Klatt and S. Huveneers, *Curr. Opin. Lipidol.*, 2022, **33**, 353–363.
36 S. A. Dabravolski, A. M. Markin, E. R. Andreeva, I. I. Eremin, A. N. Orekhov and A. A. Melnichenko, *Biomed. Pharmacother.*, 2022, **156**, 113928.
37 H. F. Galley and N. R. Webster, *Br. J. Anaesth.*, 2004, **93**, 105–113.
38 E. McEvoy, T. Sneh, E. Moeendarbary, Y. Javanmardi, N. Efimova, C. Yang, G. E. Marino-Bravante, X. Chen, J. Escribano, F. Spill, J. M. Garcia-Aznar, A. T. Weeraratna, T. M. Svitkina, R. D. Kamm and V. B. Shenoy, *Nat. Commun.*, 2022, **13**, 7089.
39 C. A. Dessalles, C. Leclech, A. Castagnino and A. I. Barakat, *Commun. Biol.*, 2021, **4**, 764.
40 I. A. Tamargo, K. I. Baek, Y. Kim, C. Park and H. Jo, *Nat. Rev. Cardiol.*, 2023, **20**, 738–753.
41 J. D. Humphrey and M. A. Schwartz, *Annu. Rev. Biomed. Eng.*, 2021, **23**, 1–27.
42 M. Marino, B. Sauty and G. Vairo, *Biomech. Model. Mechanobiol.*, 2024, **23**, 1091–1120.
43 G. Bergers and S. Song, *Neuro-Oncology*, 2005, **7**, 452–464.
44 T. Matsumoto, S. Sugita and T. Yaguchi, in *Advances in Metallic Biomaterials: Tissues, Materials and Biological Reactions*, ed. M. Niinomi, T. Narushima and M. Nakai, Springer Berlin Heidelberg, Berlin, Heidelberg, 2015, pp. 71–98, DOI: 10.1007/978-3-662-46836-4_4.
45 M. Li, M. Qian, K. Kyler and J. Xu, *Front. Cardiovasc. Med.*, 2018, **5**, 151.
46 J. Zhou, Y.-S. Li and S. Chien, *Arterioscler., Thromb., Vasc. Biol.*, 2014, **34**, 2191–2198.
47 X. Liu and Z. Bouman Chen, *eLife*, 2023, **12**, e88248.
48 D. J. Green, M. T. E. Hopman, J. Padilla, M. H. Laughlin and D. H. J. Thijssen, *Physiol. Rev.*, 2017, **97**, 495–528.
49 R. W. Colman, *J. Exp. Med.*, 2006, **203**, 493–495.
50 Y. Zhang, S.-S.-S. Aye, V. Cheng, A. Nasser, T. Hong, P. Vatankhah, F. Jiang, Y. C. Zhao, L. Moldovan, A. Sun, A. Dupuy, Y. Wang, Z. Li, T. Ang, F. Passam, K.-T. Yong and L. A. Ju, *Adv. Mater. Interfaces*, 2023, **10**, 2300234.
51 Y. C. Zhao, Y. Zhang, Z. Wang, F. Jiang, K. Kyanian, S.-S.-S. Aye, T. Hong, P. Vatankhah, A. Nasser, A. Sun, L. Moldovan, Q. P. Su, A.-N. Cho, Y. Wang, F. Passam, T. Ang and L. A. Ju, *Adv. Funct. Mater.*, 2023, **33**, 2214179.
52 C. F. Buchanan, S. S. Verbridge, P. P. Vlachos and M. N. Rylander, *Cell Adhes. Migr.*, 2014, **8**, 517–524.
53 O. Ogunrinade, G. T. Kameya and G. A. Truskey, *Ann. Biomed. Eng.*, 2002, **30**, 430–446.
54 J. M. Tarbell, *Annu. Rev. Biomed. Eng.*, 2003, **5**, 79–118.
55 J.-J. Chiu and S. Chien, *Physiol. Rev.*, 2011, **91**, 327–387.

56 R. M. Nerem, R. W. Alexander, D. C. Chappell, R. M. Medford, S. E. Varner and W. R. Taylor, *Am. J. Med. Sci.*, 1998, **316**(3), 169–175.
57 K. K. Wu and P. Thiagarajan, *Annu. Rev. Med.*, 1996, **47**, 315–331.
58 S. Baratchi, K. Khoshmanesh, O. L. Woodman, S. Potocnik, K. Peter and P. McIntyre, *Trends Mol. Med.*, 2017, **23**, 850–868.
59 T. Zhang, L. Liu, X. Huang, X. Gao, X. Huan, C. He and Y. Li, *Platelets*, 2024, **35**, 2288679.
60 A. Rana, E. Westein, B. Niego and C. E. Hagemeyer, *Front. Cardiovasc. Med.*, 2019, **6**, 141.
61 A. Chalkias, *Int. J. Mol. Sci.*, 2023, **24**, 17522.
62 G. Lippi and E. J. Favaloro, *Semin. Thromb. Hemostasis*, 2018, **44**, 239–248.
63 C. Jerjes-Sanchez, *Eur. Heart J.*, 2004, **26**, 3–4.
64 T. C. Mitchell, N. L. Feng, Y. T. Lam, P. L. Michael, M. Santos and S. G. Wise, *Tissue Eng., Part B*, 2022, **29**, 232–243.
65 K. S. Sakariassen, L. Orning and V. T. Turitto, *Future Sci. OA*, 2015, **1**, Fso30.
66 A. Andueza, S. Kumar, J. Kim, D.-W. Kang, H. L. Mumme, J. I. Perez, N. Villa-Roel and H. Jo, *Cell Rep.*, 2020, **33**, 108491.
67 S. L. Tressel, R.-P. Huang, N. Tomsen and H. Jo, *Arterioscler., Thromb., Vasc. Biol.*, 2007, **27**, 2150–2156.
68 P. Carmeliet, *Nat. Med.*, 2000, **6**, 389–395.
69 A. Lai, Y. Zhou, P. Thurgood, C. Chheang, N. Chandra Sekar, N. Nguyen, K. Peter, K. Khoshmanesh and S. Baratchi, *ACS Appl. Mater. Interfaces*, 2023, **15**, 59103–59116.
70 S. F. Vatner, J. Zhang, C. Vyzas, K. Mishra, R. M. Graham and D. E. Vatner, *Front. Physiol.*, 2021, **12**, 762437.
71 M. Marino, G. Vairo and P. Wriggers, *Curr. Pharm. Des.*, 2021, **27**, 1904–1917.
72 D. B. Camasão and D. Mantovani, *Mater. Today Bio*, 2021, **10**, 100106.
73 W. Zhang, Y. Liu and G. S. Kassab, *Am. J. Physiol.: Heart Circ. Physiol.*, 2007, **293**, H2355–H2360.
74 T. Ching, J. Vasudevan, S.-Y. Chang, H. Y. Tan, A. Sargur Ranganath, C. T. Lim, J. G. Fernandez, J. J. Ng, Y.-C. Toh and M. Hashimoto, *Small*, 2022, **18**, 2203426.
75 J. C. Kohn, M. C. Lampi and C. A. Reinhart-King, *Front. Genet.*, 2015, **6**, 112.
76 I. E. Hoefer, B. den Adel and M. J. A. P. Daemen, *Cardiovasc. Res.*, 2013, **99**, 276–283.
77 J. Huynh, N. Nishimura, K. Rana, J. M. Peloquin, J. P. Califano, C. R. Montague, M. R. King, C. B. Schaffer and C. A. Reinhart-King, *Sci. Transl. Med.*, 2011, **3**, 112ra122–112ra122.
78 E. D. Johnson, J. C. Schell and G. M. Rodgers, *Am. J. Hematol.*, 2019, **94**, 833–839.
79 R. Paniccia, R. Priora, A. A. Liotta and R. Abbate, *Vasc. Health Risk Manage.*, 2015, **11**, 133–148.
80 D. A. Gorog and R. C. Becker, *J. Thromb. Thrombolysis*, 2021, **51**, 1–11.
81 S. Pulivarthi and M. K. Gurram, *North Am. J. Med. Sci.*, 2014, **6**, 491–499.
82 L.-A. Linkins and S. Takach Lapner, *Int. J. Lab. Hematol.*, 2017, **39**, 98–103.
83 J. I. Weitz and N. C. Chan, *Arterioscler., Thromb., Vasc. Biol.*, 2019, **39**, 7–12.
84 N. Levy, *Int. J. Stroke*, 2012, **7**, 440–442.
85 J. M. Tarbell, *Cardiovasc. Res.*, 2010, **87**, 320–330.
86 C. Wang, K. Qu, J. Wang, R. Qin, B. Li, J. Qiu and G. Wang, *Biochim. Biophys. Acta, Mol. Basis Dis.*, 2022, **1868**, 166495.
87 S. Ahmed, V. M. Chauhan, A. M. Ghaemmaghami and J. W. Aylott, *Biotechnol. Lett.*, 2019, **41**, 1–25.
88 R. G. Mannino, D. R. Myers, B. Ahn, Y. Wang, R. Margo, H. Gole, A. S. Lin, R. E. Guldberg, D. P. Giddens, L. H. Timmins and W. A. Lam, *Sci. Rep.*, 2015, **5**, 12401.
89 D. R. Myers, Y. Sakurai, R. Tran, B. Ahn, E. T. Hardy, R. Mannino, A. Kita, M. Tsai and W. A. Lam, *J. Visualized Exp.*, 2012, **64**, 3958.
90 L. A. Ju, S. Kossmann, Y. C. Zhao, L. Moldovan, Y. Zhang, S. De Zoysa Ramasundara, F. Zhou, H. Lu, I. Alwis, S. M. Schoenwaelder, Y. Yuan and S. P. Jackson, *Analyst*, 2022, **147**, 1222–1235.
91 T. V. Colace, G. W. Tormoen, O. J. T. McCarty and S. L. Diamond, *Annu. Rev. Biomed. Eng.*, 2013, **15**, 283–303.
92 P. Mukherjee, F. Nebuloni, H. Gao, J. Zhou and I. Papautsky, *Micromachines*, 2019, **10**, 192.
93 A. Espinosa, J. Diaz, E. Vazquez, L. Acosta, A. Santiago and L. Cunci, *Talanta Open*, 2022, **6**, 100142.
94 N. Ansari, N. Trambadiya, A. Lodha and S. K. Menon, *Aust. J. Forensic Sci.*, 2021, **53**, 407–418.
95 P. F. Costa, H. J. Albers, J. E. A. Linssen, H. H. T. Middelkamp, L. van der Hout, R. Passier, A. van den Berg, J. Malda and A. D. van der Meer, *Lab Chip*, 2017, **17**, 2785–2792.
96 D. Khorsandi, M. Nodehi, T. Waqar, M. Shabani, B. Kamare, E. N. Zare, S. Ersoy, M. Annabestani, M. F. Çelebi and A. Kafadenk, *J. Nanomater.*, 2021, **2021**, 5537074.
97 A. Dellaquila, *Five short stories on the history of microfluidics*, ElveFlow, Paris, France, 2017.
98 M. Tsai, A. Kita, J. Leach, R. Rounsevell, J. N. Huang, J. Moake, R. E. Ware, D. A. Fletcher and W. A. Lam, *J. Clin. Invest.*, 2012, **122**, 408–418.
99 R. Barrile, A. D. van der Meer, H. Park, J. P. Fraser, D. Simic, F. Teng, D. Conegliano, J. Nguyen, A. Jain, M. Zhou, K. Karalis, D. E. Ingber, G. A. Hamilton and M. A. Otieno, *Clin. Pharmacol. Ther.*, 2018, **104**, 1240–1248.
100 A. Jain, A. Graveline, A. Waterhouse, A. Vernet, R. Flaumenhaft and D. E. Ingber, *Nat. Commun.*, 2016, **7**, 10176.
101 D. J. Luna, N. K. R. Pandian, T. Mathur, J. Bui, P. Gadangi, V. V. Kostousov, S.-K. R. Hui, J. Teruya and A. Jain, *Sci. Rep.*, 2020, **10**, 5742.
102 F. Akther, J. Zhang, H. D. N. Tran, H. Fallahi, H. Adelnia, H.-P. Phan, N.-T. Nguyen and H. T. Ta, *Adv. Biol.*, 2022, **6**, 2270071.

103 A. M. Iqbal, R. A. Lopez and O. Hai, in *StatPearls*, StatPearls Publishing Copyright ©, 2024, StatPearls Publishing LLC., Treasure Island (FL), 2024.
104 C. Kearon and E. A. Akl, *Blood*, 2014, **123**, 1794–1801.
105 D. C. Duffy, J. C. McDonald, O. J. A. Schueller and G. M. Whitesides, *Anal. Chem.*, 1998, **70**, 4974–4984.
106 F. Akther, H. Fallahi, J. Zhang, N.-T. Nguyen and H. T. Ta, *Lab Chip*, 2024, **24**, 2927–2943.
107 A. Jain, R. Barrile, A. van der Meer, A. Mammoto, T. Mammoto, K. De Ceunynck, O. Aisiku, M. Otieno, C. Louden, G. Hamilton, R. Flaumenhaft and D. Ingber, *Clin. Pharmacol. Ther.*, 2018, **103**, 332–340.
108 A. Dupuy, L. Hagimola, N. S. A. Mgaieth, C. B. Houlahan, R. E. Preketes-Tardiani, P. R. Coleman and F. H. Passam, *Diagnostics*, 2021, **11**, 203.
109 K.-T. Liu, P.-W. Wang, H.-Y. Hsieh, H.-C. Pan, H.-J. Chin, C.-W. Lin, Y.-J. Huang, Y.-C. Liao, Y.-C. Tsai, S.-R. Liu, I. C. Su, Y.-F. Song, G.-C. Yin, K.-C. Wu, E.-Y. Chuang, Y.-J. Fan and J. Yu, *Lab Chip*, 2024, **24**, 3422–3433.
110 U. M. Sonmez, Y.-W. Cheng, S. C. Watkins, B. L. Roman and L. A. Davidson, *Lab Chip*, 2020, **20**, 4373–4390.
111 K. M. Stroka and H. Aranda-Espinoza, *Blood*, 2011, **118**, 1632–1640.
112 P. A. Galie, A. van Oosten, C. S. Chen and P. A. Janmey, *Lab Chip*, 2015, **15**, 1205–1212.
113 C. Xue, T. Zhang, X. Xie, Q. Zhang, S. Zhang, B. Zhu, Y. Lin and X. Cai, *Biochim. Biophys. Acta, Mol. Cell Res.*, 2017, **1864**, 1799–1808.
114 F. Akther, S. B. Yakob, N.-T. Nguyen and H. T. Ta, *Biosensors*, 2020, **10**, 182.
115 D. Bodas and C. Khan-Malek, *Sens. Actuators, B*, 2007, **123**, 368–373.
116 D. Fuard, T. Tzvetkova-Chevolleau, S. Decossas, P. Tracqui and P. Schiavone, *Microelectron. Eng.*, 2008, **85**, 1289–1293.
117 X. Y. Wang, C. Fillafer, C. Pichl, S. Deinhammer, R. Hofer-Warbinek, M. Wirth and F. Gabor, *Biomicrofluidics*, 2013, **7**, 44127.
118 Y. Hong, I. Koh, K. Park and P. Kim, *ACS Biomater. Sci. Eng.*, 2017, **3**, 3546–3552.
119 L. Rao, Y. Liu and H. Zhou, *J. Mater. Sci.: Mater. Med.*, 2022, **33**, 66.
120 S. Khetani, K. W. Yong, V. Ozhukil Kollath, E. Eastick, M. Azarmanesh, K. Karan, A. Sen and A. Sanati-Nezhad, *ACS Appl. Mater. Interfaces*, 2020, **12**, 6910–6923.
121 R. Sfriso, S. Zhang, C. A. Bichsel, O. Steck, A. Despont, O. T. Guenat and R. Rieben, *Sci. Rep.*, 2018, **8**, 5898.
122 X. Li, Q. Sun, Q. Li, N. Kawazoe and G. Chen, *Front. Chem.*, 2018, **6**, 499.
123 W. Wang, L. Guo, Y. Yu, Z. Chen, R. Zhou and Z. Yuan, *J. Biomed. Mater. Res., Part A*, 2015, **103**, 1703–1712.
124 D. Hao, R. Liu, K. Gao, C. He, S. He, C. Zhao, G. Sun, D. L. Farmer, A. Panitch, K. S. Lam and A. Wang, *Front. Bioeng. Biotechnol.*, 2020, **8**, 890.
125 L. J. Taite, M. L. Rowland, K. A. Ruffino, B. R. E. Smith, M. B. Lawrence and J. L. West, *Ann. Biomed. Eng.*, 2006, **34**, 1705–1711.
126 S.-S. S. Aye, R. Li, M. Boyd-Moss, B. Long, S. Pavuluri, K. Bruggeman, Y. Wang, C. R. Barrow, D. R. Nisbet and R. J. Williams, *Polymers*, 2018, **10**, 690.
127 K. H. Song, C. B. Highley, A. Rouff and J. A. Burdick, *Adv. Funct. Mater.*, 2018, **28**, 1801331.
128 C. B. Goy, R. E. Chaile and R. E. Madrid, *React. Funct. Polym.*, 2019, **145**, 104314.
129 H.-J. Koo and O. D. Velev, *Biomicrofluidics*, 2017, **11**, 024104.
130 I. D. Orge, H. Nogueira Pinto, M. A. Silva, S. J. Bidarra, S. A. Ferreira, I. Calejo, R. Masereeuw, S. M. Mihăilă and C. C. Barrias, *Bioact. Mater.*, 2024, **38**, 499–511.
131 J. A. Whisler, M. B. Chen and R. D. Kamm, *Tissue Eng., Part C*, 2014, **20**, 543–552.
132 B. Carrion, C. P. Huang, C. M. Ghajar, S. Kachgal, E. Kniazeva, N. L. Jeon and A. J. Putnam, *Biotechnol. Bioeng.*, 2010, **107**, 1020–1028.
133 G. M. Price, K. H. K. Wong, J. G. Truslow, A. D. Leung, C. Acharya and J. Tien, *Biomaterials*, 2010, **31**, 6182–6189.
134 D.-H. T. Nguyen, S. C. Stapleton, M. T. Yang, S. S. Cha, C. K. Choi, P. A. Galie and C. S. Chen, *Proc. Natl. Acad. Sci. U. S. A.*, 2013, **110**, 6712–6717.
135 R. M. Linville, N. F. Boland, G. Covarrubias, G. M. Price and J. Tien, *Cell. Mol. Bioeng.*, 2016, **9**, 73–84.
136 H. H. G. Song, R. T. Rumma, C. K. Ozaki, E. R. Edelman and C. S. Chen, *Cell Stem Cell*, 2018, **22**, 340–354.
137 C. Shen, Y. Li, Y. Wang and Q. Meng, *Lab Chip*, 2019, **19**, 3962–3973.
138 J. H. Park, B. G. Chung, W. G. Lee, J. Kim, M. D. Brigham, J. Shim, S. Lee, C. M. Hwang, N. G. Durmus, U. Demirci and A. Khademhosseini, *Biotechnol. Bioeng.*, 2010, **106**, 138–148.
139 K. M. Chrobak, D. R. Potter and J. Tien, *Microvasc. Res.*, 2006, **71**, 185–196.
140 Q. Vo, K. A. Carlson, P. M. Chiknas, C. N. Brocker, L. DaSilva, E. Clark, S. K. Park, A. S. Ajiboye, E. M. Wier and K. H. Benam, *Adv. Funct. Mater.*, 2024, **34**, 2304630.
141 R. G. Mannino, A. N. Santiago-Miranda, P. Pradhan, Y. Qiu, J. C. Mejias, S. S. Neelapu, K. Roy and W. A. Lam, *Lab Chip*, 2017, **17**, 407–414.
142 S. Zhao, Y. Chen, B. P. Partlow, A. S. Golding, P. Tseng, J. Coburn, M. B. Applegate, J. E. Moreau, F. G. Omenetto and D. L. Kaplan, *Biomaterials*, 2016, **93**, 60–70.
143 X.-Y. Wang, Z.-H. Jin, B.-W. Gan, S.-W. Lv, M. Xie and W.-H. Huang, *Lab Chip*, 2014, **14**, 2709–2716.
144 A. Mora-Boza, A. Mulero-Russe, N. D. Caprio, J. A. Burdick, A. Singh and A. J. Garcia, *Adv. Mater.*, 2023, **35**, e2306765.
145 B. M. Gillette, J. A. Jensen, B. Tang, G. J. Yang, A. Bazargan-Lari, M. Zhong and S. K. Sia, *Nat. Mater.*, 2008, **7**, 636–640.
146 A. Mora-Boza, A. Mulero-Russe, N. D. Caprio, J. A. Burdick, A. Singh and A. J. García, *Adv. Mater.*, 2023, **35**, 2306765.
147 C. Arakawa, C. Gunnarsson, C. Howard, M. Bernabeu, K. Phong, E. Yang, C. A. DeForest, J. D. Smith and Y. Zheng, *Sci. Adv.*, 2020, **6**, eaay7243.

148 H. F. Dvorak, L. F. Brown, M. Detmar and A. M. Dvorak, *Am. J. Pathol.*, 1995, **146**, 1029–1039.
149 S. Xu, I. Ilyas, P. J. Little, H. Li, D. Kamato, X. Zheng, S. Luo, Z. Li, P. Liu, J. Han, I. C. Harding, E. E. Ebong, S. J. Cameron, A. G. Stewart and J. Weng, *Pharmacol. Rev.*, 2021, **73**, 924.
150 J. D. Allbritton-King and G. García-Cardeña, *Front. Cell Dev. Biol.*, 2023, **11**, 1278166.
151 H. A. Hadi and J. A. Suwaidi, *Vasc. Health Risk Manage.*, 2007, **3**, 853–876.
152 M. Dubsky, J. Veleba, D. Sojakova, N. Marhefkova, V. Fejfarova and E. B. Jude, *Int. J. Mol. Sci.*, 2023, **24**, 10705.
153 J. Hanson, S. J. Lee, M. A. Hossain, N. M. Anstey, P. Charunwatthana, R. J. Maude, H. W. F. Kingston, S. K. Mishra, S. Mohanty, K. Plewes, K. Piera, M. U. Hassan, A. Ghose, M. A. Faiz, N. J. White, N. P. J. Day and A. M. Dondorp, *BMC Med.*, 2015, **13**, 122.
154 M. A. Bush, N. M. Anstey, T. W. Yeo, S. M. Florence, D. L. Granger, E. D. Mwaikambo and J. B. Weinberg, *Front. Cell Dev. Biol.*, 2021, **9**, 751251.
155 N. R. Machado, K. T. Dias, B. F. S. Cortes and S. F. Rodrigues, *Ther. Adv. Respir. Dis.*, 2023, **17**, 17534666231162252.
156 M. Wang, J. Feng, D. Zhou and J. Wang, *Eur. J. Med. Res.*, 2023, **28**, 339.
157 S. P. S. Dhami, S. Patmore, C. Comerford, C. M. Byrne, B. Cavanagh, J. Castle, C. C. Kirwan, M. Kenny, I. Schoen, J. S. O'Donnell and J. M. O'Sullivan, *J. Thromb. Haemostasis*, 2022, **20**, 2350–2365.
158 H. Ehlers, A. Nicolas, F. Schavemaker, J. P. M. Heijmans, M. Bulst, S. J. Trietsch and L. J. van den Broek, *Front. Immunol.*, 2023, **14**, 1118624.
159 J.-L. Knop, N. Burkard, M. Danesh, S. Kintrup, T. Dandekar, M. Srivastava, R. Springer, M. Hiermaier, N.-M. Wagner, J. Waschke, S. Flemming and N. Schlegel, *iScience*, 2023, **26**, 108049.
160 H. F. Langer and T. Chavakis, *J. Cell. Mol. Med.*, 2009, **13**, 1211–1220.
161 W. A. Muller, *Lab. Invest.*, 2002, **82**, 521–534.
162 A. Shamloo, N. Ma, M.-m. Poo, L. L. Sohn and S. C. Heilshorn, *Lab Chip*, 2008, **8**, 1292–1299.
163 D. Sarmah, M. Borah, M. Mandal and N. Karak, *J. Mater. Chem. B*, 2023, **11**, 2927–2936.
164 M. Tavakolian, J. G. Munguia-Lopez, A. Valiei, M. S. Islam, J. M. Kinsella, N. Tufenkji and T. G. M. van de Ven, *ACS Appl. Mater. Interfaces*, 2020, **12**, 39991–40001.
165 W. Feng and Z. Wang, *Adv. Sci.*, 2023, **10**, 2303326.
166 H. Li, H. Wang, D. Zhang, Z. Xu and W. Liu, *Polymer*, 2018, **153**, 193–200.
167 X. Li, H. Wang, D. Li, S. Long, G. Zhang and Z. Wu, *ACS Appl. Mater. Interfaces*, 2018, **10**, 31198–31207.
168 S. Li, D. Zhou, M. Pei, Y. Zhou, W. Xu and P. Xiao, *Eur. Polym. J.*, 2020, **134**, 109854.
169 J. W. Nichol, S. T. Koshy, H. Bae, C. M. Hwang, S. Yamanlar and A. Khademhosseini, *Biomaterials*, 2010, **31**, 5536–5544.
170 Q. Zhou, K. Yang, J. He, H. Yang and X. Zhang, *J. Mater. Chem. C*, 2019, **7**, 14913–14922.
171 J. Zheng, S. Jung, P. W. Schmidt, T. P. Lodge and T. M. Reineke, *ACS Macro Lett.*, 2017, **6**, 145–149.
172 T. B. Becher and C. Ornelas, *ChemistrySelect*, 2017, **2**, 3009–3013.
173 F. Jia, J. M. Kubiak, M. Onoda, Y. Wang and R. J. Macfarlane, *Adv. Sci.*, 2021, **8**, 2100968.
174 Y. Zhan, W. Fu, Y. Xing, X. Ma and C. Chen, *Mater. Sci. Eng., C*, 2021, **127**, 112208.
175 L. J. Macdougall, M. M. Pérez-Madrigal, M. C. Arno and A. P. Dove, *Biomacromolecules*, 2018, **19**, 1378–1388.
176 T. Sakai, T. Matsunaga, Y. Yamamoto, C. Ito, R. Yoshida, S. Suzuki, N. Sasaki, M. Shibayama and U.-i. Chung, *Macromolecules*, 2008, **41**, 5379–5384.
177 Y. Ling, J. Rubin, Y. Deng, C. Huang, U. Demirci, J. M. Karp and A. Khademhosseini, *Lab Chip*, 2007, **7**, 756–762.
178 W. J. Polacheck, M. L. Kutys, J. Yang, J. Eyckmans, Y. Wu, H. Vasavada, K. K. Hirschi and C. S. Chen, *Nature*, 2017, **552**, 258–262.
179 K. H. K. Wong, J. G. Truslow and J. Tien, *Biomaterials*, 2010, **31**, 4706–4714.
180 K. A. Heintz, M. E. Bregenzer, J. L. Mantle, K. H. Lee, J. L. West and J. H. Slater, *Adv. Healthcare Mater.*, 2016, **5**, 2153–2160.
181 D. Wang, S. Maharjan, X. Kuang, Z. Wang, L. S. Mille, M. Tao, P. Yu, X. Cao, L. Lian, L. Lv, J. J. He, G. Tang, H. Yuk, C. K. Ozaki, X. Zhao and Y. S. Zhang, *Sci. Adv.*, 2022, **8**, eabq6900.
182 Y. S. Zhang, F. Davoudi, P. Walch, A. Manbachi, X. Luo, V. Dell'Erba, A. K. Miri, H. Albadawi, A. Arneri, X. Li, X. Wang, M. R. Dokmeci, A. Khademhosseini and R. Oklu, *Lab Chip*, 2016, **16**, 4097–4105.
183 R. Levato, K. S. Lim, W. Li, A. U. Asua, L. B. Peña, M. Wang, M. Falandt, P. N. Bernal, D. Gawlitta, Y. S. Zhang, T. B. F. Woodfield and J. Malda, *Mater. Today Bio*, 2021, **12**, 100162.
184 G. Größbacher, M. Bartolf-Kopp, C. Gergely, P. N. Bernal, S. Florczak, M. de Ruijter, N. G. Rodriguez, J. Groll, J. Malda, T. Jungst and R. Levato, *Adv. Mater.*, 2023, **35**, 2300756.
185 J. Gehlen, W. Qiu, G. N. Schädli, R. Müller and X.-H. Qin, *Acta Biomater.*, 2023, **156**, 49–60.
186 I. S. Kinstlinger, S. H. Saxton, G. A. Calderon, K. V. Ruiz, D. R. Yalacki, P. R. Deme, J. E. Rosenkrantz, J. D. Louis-Rosenberg, F. Johansson, K. D. Janson, D. W. Sazer, S. S. Panchavati, K.-D. Bissig, K. R. Stevens and J. S. Miller, *Nat. Biomed. Eng.*, 2020, **4**, 916–932.
187 B. Grigoryan, S. J. Paulsen, D. C. Corbett, D. W. Sazer, C. L. Fortin, A. J. Zaita, P. T. Greenfield, N. J. Calafat, J. P. Gounley, A. H. Ta, F. Johansson, A. Randles,

J. E. Rosenkrantz, J. D. Louis-Rosenberg, P. A. Galie, K. R. Stevens and J. S. Miller, *Science*, 2019, **364**, 458–464.
188 R. Attalla, C. Ling and P. Selvaganapathy, *Biomed. Microdevices*, 2016, **18**, 17.
189 R. Rizzo, D. Ruetsche, H. Liu and M. Zenobi-Wong, *Adv. Mater.*, 2021, **33**, 2102900.
190 W. Li, M. Wang, L. S. Mille, J. A. Robledo Lara, V. Huerta, T. Uribe Velázquez, F. Cheng, H. Li, J. Gong, T. Ching, C. A. Murphy, A. Lesha, S. Hassan, T. B. F. Woodfield, K. S. Lim and Y. S. Zhang, *Adv. Mater.*, 2021, **33**, 2102153.
191 C. Colosi, S. R. Shin, V. Manoharan, S. Massa, M. Costantini, A. Barbetta, M. R. Dokmeci, M. Dentini and A. Khademhosseini, *Adv. Mater.*, 2016, **28**, 677–684.
192 Q. Gao, Y. He, J.-z. Fu, A. Liu and L. Ma, *Biomaterials*, 2015, **61**, 203–215.
193 J. Simińska-Stanny, L. Nicolas, A. Chafai, H. Jafari, M. Hajiabbas, G. Dodi, I. Gardikiotis, C. Delporte, L. Nie, D. Podstawczyk and A. Shavandi, *Bioact. Mater.*, 2024, **36**, 168–184.
194 Q. Gao, Y. He, J. Z. Fu, A. Liu and L. Ma, *Biomaterials*, 2015, **61**, 203–215.
195 T. Bhattacharjee, S. M. Zehnder, K. G. Rowe, S. Jain, R. M. Nixon, W. G. Sawyer and T. E. Angelini, *Sci. Adv.*, 2015, **1**, e1500655.
196 T. J. Hinton, Q. Jallerat, R. N. Palchesko, J. H. Park, M. S. Grodzicki, H.-J. Shue, M. H. Ramadan, A. R. Hudson and A. W. Feinberg, *Sci. Adv.*, 2015, **1**, e1500758.
197 A. McCormack, C. B. Highley, N. R. Leslie and F. P. W. Melchels, *Trends Biotechnol.*, 2020, **38**, 584–593.
198 H. Kim, J. Jang, J. Park, K.-P. Lee, S. Lee, D.-M. Lee, K. H. Kim, H. K. Kim and D.-W. Cho, *Biofabrication*, 2019, **11**, 035017.
199 H.-Q. Xu, J.-C. Liu, Z.-Y. Zhang and C.-X. Xu, *Mil. Med. Res.*, 2022, **9**, 70.
200 D. B. Kolesky, K. A. Homan, M. A. Skylar-Scott and J. A. Lewis, *Proc. Natl. Acad. Sci. U. S. A.*, 2016, **113**, 3179–3184.
201 S. M. Hull, L. G. Brunel and S. C. Heilshorn, *Adv. Mater.*, 2022, **34**, 2103691.
202 G. Gao, W. Park, B. S. Kim, M. Ahn, S. Chae, W.-W. Cho, J. Kim, J. Y. Lee, J. Jang and D.-W. Cho, *Adv. Funct. Mater.*, 2021, **31**, 2008878.
203 L. E. Bertassoni, M. Cecconi, V. Manoharan, M. Nikkhah, J. Hjortnaes, A. L. Cristino, G. Barabaschi, D. Demarchi, M. R. Dokmeci, Y. Yang and A. Khademhosseini, *Lab Chip*, 2014, **14**, 2202–2211.
204 W. F. Hynes, M. Pepona, C. Robertson, J. Alvarado, K. Dubbin, M. Triplett, J. J. Adorno, A. Randles and M. L. Moya, *Sci. Adv.*, 2020, **6**, eabb3308.
205 R. E. B. Fitzsimmons, M. S. Aquilino, J. Quigley, O. Chebotarev, F. Tarlan and C. A. Simmons, *Bioprinting*, 2018, **9**, 7–18.
206 L. Ouyang, J. P. K. Armstrong, Q. Chen, Y. Lin and M. M. Stevens, *Adv. Funct. Mater.*, 2020, **30**, 1908349.
207 W. Wu, A. DeConinck and J. A. Lewis, *Adv. Mater.*, 2011, **23**, H178–H183.
208 D. B. Kolesky, K. A. Homan, M. A. Skylar-Scott and J. A. Lewis, *Proc. Natl. Acad. Sci. U. S. A.*, 2016, **113**, 3179–3184.
209 K. Yu, X. Zhang, Y. Sun, Q. Gao, J. Fu, X. Cai and Y. He, *Bioact. Mater.*, 2022, **11**, 254–267.
210 A. Bhusal, E. Dogan, H.-A. Nguyen, O. Labutina, D. Nieto, A. Khademhosseini and A. K. Miri, *Biofabrication*, 2022, **14**, 014103.
211 B. E. Kelly, I. Bhattacharya, H. Heidari, M. Shusteff, C. M. Spadaccini and H. K. Taylor, *Science*, 2019, **363**, 1075–1079.
212 Q. Thijssen, A. Quaak, J. Toombs, E. De Vlieghere, L. Parmentier, H. Taylor and S. Van Vlierberghe, *Adv. Mater.*, 2023, **35**, 2210136.
213 J. Madrid-Wolff, J. Toombs, R. Rizzo, P. N. Bernal, D. Porcincula, R. Walton, B. Wang, F. Kotz-Helmer, Y. Yang, D. Kaplan, Y. S. Zhang, M. Zenobi-Wong, R. R. McLeod, B. Rapp, J. Schwartz, M. Shusteff, H. Talyor, R. Levato and C. Moser, *MRS Commun.*, 2023, **13**, 764–785.
214 M. Falandt, P. N. Bernal, O. Dudaryeva, S. Florczak, G. Größbacher, M. Schweiger, A. Longoni, C. Greant, M. Assunção, O. Nijssen, S. van Vlierberghe, J. Malda, T. Vermonden and R. Levato, *Adv. Mater. Technol.*, 2023, **8**, 2300026.
215 J. W. Seo, G. M. Kim, Y. Choi, J. M. Cha and H. Bae, *Int. J. Mol. Sci.*, 2022, **23**, 5428.
216 S. You, Y. Xiang, H. H. Hwang, D. B. Berry, W. Kiratitanaporn, J. Guan, E. Yao, M. Tang, Z. Zhong, X. Ma, D. Wangpraseurt, Y. Sun, T.-y. Lu and S. Chen, *Sci. Adv.*, 2023, **9**, eade7923.
217 K. Elkhoury, J. Zuazola and S. Vijayavenkataraman, *SLAS Technol.*, 2023, **28**, 142–151.
218 P. P. Stankey, K. T. Kroll, A. J. Ainscough, D. S. Reynolds, A. Elamine, B. T. Fichtenkort, S. G. M. Uzel and J. A. Lewis, *Adv. Mater.*, 2024, **36**, 2401528.
219 Y. He, Z. Gu, M. Xie, J. Fu and H. Lin, *Bio-Des. Manuf.*, 2020, **3**, 1–4.
220 T. Ching, J. Vasudevan, S.-Y. Chang, H. Y. Tan, C. T. Lim, J. G. Fernandez, J. J. Ng, Y.-C. Toh and M. Hashimoto, *bioRxiv*, 2021, preprint, DOI: **10.1101/2021.09.27.461981**, 2021.2009.2027.461981.
221 Z. Zeng, C. Hu, Q. Liang, L. Tang, D. Cheng and C. Ruan, *Bioact. Mater.*, 2021, **6**, 1628–1638.
222 W. Meyer, S. Engelhardt, E. Novosel, B. Elling, M. Wegener and H. Krüger, *J. Funct. Biomater.*, 2012, **3**, 257–268.
223 W. Qiu, J. Gehlen, M. Bernero, C. Gehre, G. N. Schädli, R. Müller and X.-H. Qin, *Adv. Funct. Mater.*, 2023, **33**, 2214393.
224 R. Abbasi, T. B. LeFevre, A. D. Benjamin, I. J. Thornton and J. N. Wilking, *Lab Chip*, 2021, **21**, 2050–2058.
225 B. J. O'Grady, J. X. Wang, S. L. Faley, D. A. Balikov, E. S. Lippmann and L. M. Bellan, *SLAS Technol.*, 2018, **23**, 592–598.

226 E. E. van Haaften, T. B. Wissing, M. C. M. Rutten, J. A. Bulsink, K. Gashi, M. A. J. van Kelle, A. I. P. M. Smits, C. V. C. Bouten and N. A. Kurniawan, *Tissue Eng., Part C*, 2018, **24**, 418–429.

227 N. Salehi-Nik, G. Amoabediny, B. Pouran, H. Tabesh, M. A. Shokrgozar, N. Haghighipour, N. Khatibi, F. Anisi, K. Mottaghy and B. Zandieh-Doulabi, *BioMed Res. Int.*, 2013, **2013**, 762132.